• U C •

FCTUC FACULDADE DE CIÊNCIAS
E TECNOLOGIA
UNIVERSIDADE DE COIMBRA

DEPARTAMENTO DE
ENGENHARIA MECÂNICA

Optimization of the flow in a dipping tank using CFD

Submitted in Partial Fulfilment of the Requirements for the Degree of Master in Mechanical Engineering in the speciality of Energy and Environment

Otimização, através de CFD, do escoamento num tanque de imersão

Author

André Micael Cardoso Ferreira

Advisors

Almerindo Domingues Ferreira

João Carlos Queimadela Bento

Jury

President	**Professor Doutor Pedro de Figueiredo Vieira Carvalheira** **Professor da Universidade de Coimbra**
Vowel	**Professor Doutor António Manuel Gameiro Lopes** **Professor da Universidade de Coimbra**
Advisor	**Professor Doutor Almerindo Domingues Ferreira** **Professor da Universidade de Coimbra**

Institutional Collaboration

Ansell **Ansell**

Coimbra, September, 2018

Aquele mar
meu confidente de horas idas
tudo escutava e adivinhava
do meu pueril e ingénuo anseio.

João de Barros

AGRADECIMENTOS

Durante a realização deste trabalho surgiu o apoio de pessoas que, sem as quais, este não existiria. Em primeiro lugar um agradecimento especial aos orientadores. Ao Professor Doutor Almerindo Ferreira pelo acompanhamento incondicional, pelas oportunidades e bem-estar fornecido durante os meses de trabalho desenvolvido. Ao Engenheiro João Bento, também, pela possibilidade de trabalhar inserido numa equipa dentro de uma empresa como a Ansell, pelo convívio e confiança depositada.

Não seria também possível chegar a este ponto sem a ajuda da família. À minha mãe, Adélia, em especial, pelo sacrifício ao longo de vários anos de modo a possibilitar o ingresso no ensino superior, pelos conselhos nem sempre seguidos e apoio nos piores momentos, deixo um carinho especial. Aos meus avós deixo outro, por estarem sempre presentes, mesmo quando não parece.

Ao João Miravall, por sempre me ter erguido quando a situação não era a melhor, pelos incríveis conselhos, pela motivação constante, agradeço com muito carinho. Também ao Rui e à Isa, pelo companheirismo ao longo de 5 anos, pelos jantares e por todos os momentos alegres e tristes que vivemos juntos, obrigado. Agradeço, finalmente, a todos os restantes amigos não mencionados que, mesmo com a minha ausência, nunca me esqueceram e deixaram.

Abstract

With this work, using CFD software OpenFOAM®, it is intended the simulation of the flow inside immersion tanks used in the manufacturing of protection gloves. An initial validation of the numerical model is made, adapting several parameters to approximate simulation results to real data. To improve the flow and minimize the number of rejected gloves, several deflector geometries are studied and implemented in the simulations.

Keywords CFD, flow improvement, free surface, interFOAM, jet flutter, OpenFOAM.

Resumo

Com este trabalho pretende-se simular, usando o programa de CFD OpenFOAM®, o escoamento no interior de tinas de imersão usadas no fabrico de luvas. Uma validação inicial do modelo usado é feita, alterando diferentes parâmetros de modo a ajustar os resultados das simulações a dados reais. Seguidamente, de modo a melhorar o escoamento dentro dessas tinas e minimizar o número de luvas rejeitadas, são estudadas e implementadas várias geometrias de defletores nas simulações.

Palavras-chave: CFD, interFOAM, melhoria de escoamento, OpenFOAM, oscilação de jato, superfície livre.

Contents

LIST OF FIGURES

LIST OF TABLES

1. INTRODUCTION

1.1. Motivation

The present work aims to contribute for the solve of a manufacturing problem that occurs at the company Ansell Portugal, which is based in Vila Nova de Poiares. This company manufactures protection gloves. Some of them are coated with rubber. This coating is made by diving the gloves into a rubber mixture, inside an immersion tank. They are kept there enough time for the rubber to stick at the glove's surface. The immersion tanks are composed with an entry located at the bottom. The fluid flow pumped exits from the tanks through spillways at the laterals.

Figure 1.1. Example of free surface shape at a tank of the company.

At the coating process there are rejects. These happen because, when the inlet flow is too high, a swell appears in the free surface, as seen at Figure 1.1. In some tanks, the swell oscillates. This oscillation creates waves that propagate to the spillways, which might originate gloves with different coated zones, generating a quality problem. On the other hand, when the flow rate is low, it is obtained a flat free surface, but there appear darker spots, composed of drier rubber that drops from the gloves, and float, when they are taken off the tank. These spots must be eliminated so that the next set of gloves do not incorporate them on the coating. These two problems are to be solved, in order to achieve a good mixing of the rubber and maintaining a flat free surface.

1.2. OpenFOAM®

To study the flow, it is proposed to numerically simulate the case using the software OpenFOAM® (Open Source Field Operation and Manipulation). That software was created in early 1990's. Its code is written in C++, to substitute Fortran programs made by that time. There is no consistent public opinion on who is the author of the software's code. Nevertheless, nowadays there are three main distributions of OpenFOAM®. One is led by The OpenFOAM® Foundation (https://openfoam.org/) and another by OpenCFD Ltd (ESI Group, https://openfoam.com/). There is also a project called foam-extend, where can be found community contributed extensions. This software works mainly in Linux machines.

In OpenFOAM® a case is mounted into a folder. As seen in Figure 1.2, the main folder has "time" (*0*), *constant* and *system* folders inside. The directory *constant* contains information about the mesh and physical properties. In the directory *system*, are specified parameters concerning the solving process, such as parameters for data output, time step, discretization schemes or convergence criteria. The initial directory is used to store boundary and initial conditions or results, for example, pressure and velocity fields. The text files must be manually edited, following the OpenFOAM® User Guide.

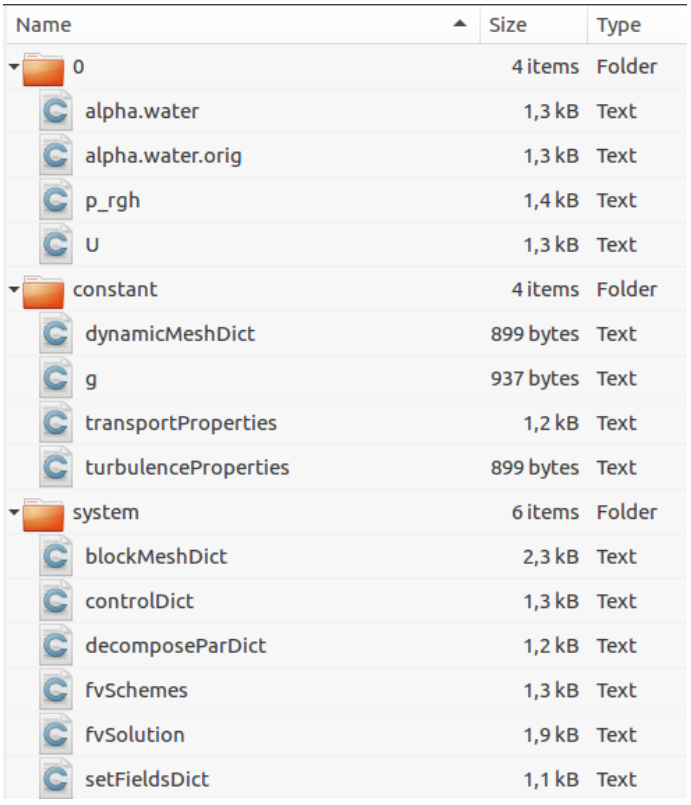

Figure 1.2. Directory tree of damBreak laminar tutorial.

So, compared with other CFD software, OpenFOAM® is more difficult to use. But it has great advantages. It's a free software, which in a company can generate tens of thousands of euros in savings, a year. Its code is open source, which means that anyone can change it, add new solvers and test their original code. Also, OpenFOAM® has a very active community. As said before, foam-extend is an example of community contributions. Also, there are several forums online (eg. https://www.cfd-online.com/Forums/openfoam/ or https://openfoamwiki.net/) where users discuss several issues regarding this software.

The present work was made using version 4.1 of the OpenFOAM®.

1.3. Bibliographic review

When a vertical plane jet, in a shallow water situation, interacts with the free surface, there appear several zones in the jet, as shown in Figure 1.3 (Kuang et al., 2001). When the jet exits from the nozzle, it forms the zone of flow establishment, then the zone of established flow. When the vertical velocity of the jet is highly decreased, and it meets the free surface, there is the zone of surface impingement. The flow that impinges on free surface, escapes to the laterals, forming horizontal jets. This last zone is the zone of horizontal jets. Kuang et al. (2001) also confirm that, besides the vertical jet, and under the zone of horizontal jets, there is the tendency to the development of recirculation cells, as it will be seen later.

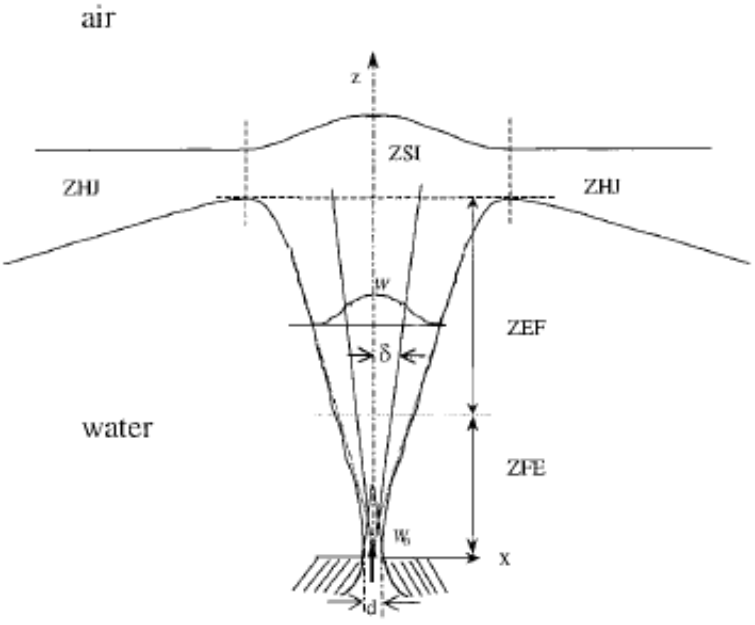

Figure 1.3. Different zones in a vertical turbulent plane jet (Kuang et al., 2001).

Also concerning vertical plane jets, Wu et al (1998) proved that, in a rectangular tank, a jet starts to flap if its velocity at the nozzle is above a certain critical value. Below that velocity, the jet does not oscillate. This critical value depends on the distance between the free surface and the jet nozzle, also on the nozzle's width. The oscillation of the jet is characterized by a certain frequency, which is a function of the nozzle's depth, in general. Only for low values of the depth, Wu et al (1998) found that frequency also varies with inlet velocity.

The movement of the jet can be caused by two factors, self-induced sloshing and jet flutter. A growth model for the first factor was proposed by Fukaya et al. (1996). According to that model, there is a feedback loop, in which the sloshing of the free surface creates a fluctuating pressure field. This fluctuation in pressure origins the oscillation of the jet, that provides energy back to the sloshing. Jet-flutter (Madarame and Iida, 1998) is caused by the swell created by the jet impingement. When the jet moves, fluid is provided to the front of the swell, which creates a low pressure there, and higher pressure at the rear. Such pressure difference contributes to the movement of the jet, which also origins a loop, oscillating the jet back and forward.

For a round jet, sloshing also occurs for a certain limit inlet velocity (Madarame at al., 2002). It also depends on the distance between the nozzle and the free surface. The main mechanism those authors found was jet-flutter.

In all the situations above mentioned, regarding jet oscillation, the fluid is bounded by walls tall enough to prevent overflow. In the paper by Espa and Frattini (2002), the experimental model with weirs at the laterals resembles more the tanks of Ansell. Those authors concluded, for their experimental model, several phenomena already described, such as swell occurrence as inlet jet velocity is increased and the critical value for the previous velocity, determining the oscillation of the jet at a certain frequency.

Espa and Frattini (2002), for several values of inlet flow rate, measured frequency by timing one hundred complete oscillations. From their results, they choose three different inlet flow rates, to further detail their investigation. This was made by using dye flow visualization, LDA velocity measurements and Fourier analysis.

Attending the relative similarity between the experimental model to the Ansell tanks, variety of results and the lack of investigations using 3D models, the paper Espa and Frattini (2002) shall be used to validate the results provided by OpenFOAM.

2. VALIDATION

2.1. Case setup

2.1.1. Geometry

In Espa and Frattini (2002), water is the fluid of their choice, so, an incompressible fluid. Also, thermal energy transfer is neglected and it is a case of two-phase flow (water and air). Regarding these specifications, and consulting the OpenFOAM user Guide, it is chosen the standard solver *interFoam* to model such problem.

To start using OpenFOAM it is suggested to pick a tutorial and then make the modifications needed. For this work, it was chosen the damBreak laminar tutorial as starting point.

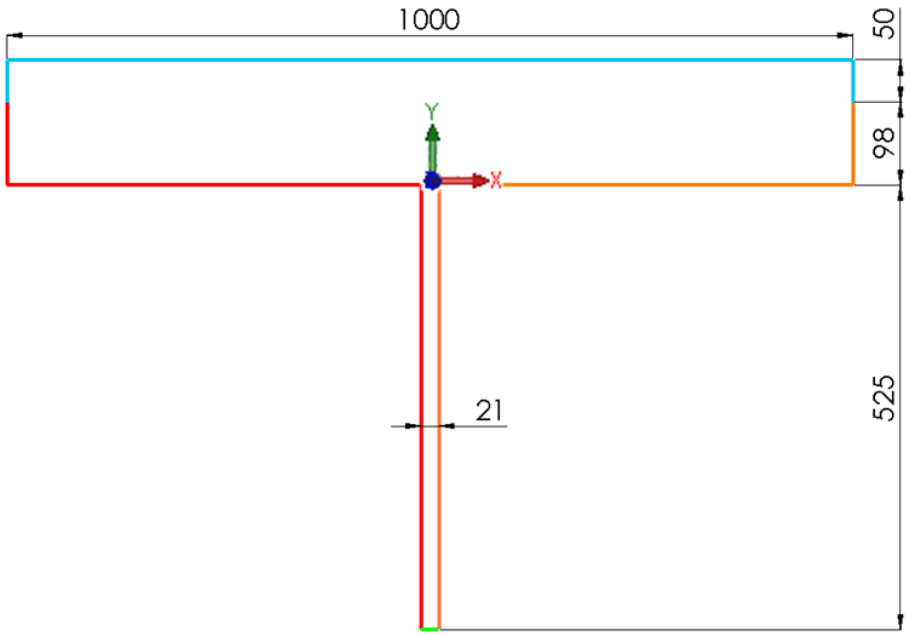

Figure 2.1. Boundaries and dimensions (in mm) of the case studied by Espa and Frattini (2002).

The geometry of the experimental model used by those authors was replicated, using the CAD software SOLIDWORKS®. Figure 2.1 shows the four surfaces created. In blue is the outlet, in red the left wall, in orange the right wall and in green the inlet, with the origin located at the centre of the entrance. All these were exported to *stl* format. Dimensions

are shown at the same figure, being the geometry symmetric to Oy axis and with a depth of 21 mm in order to have a square entrance tube (which is irrelevant for a 2D problem).

Tube length was approximated by equation (2.1) (Auld and Srinivas, 1995) in order to ensure a fully developed flow at the entrance of the tank.

$$\frac{L_e}{D} \approx 4.4 Re_D^{1/6}. \quad (2.1)$$

The entrance diameter is 21 millimetres. For Reynolds number, it was used the higher one that Espa and Frattini (2002) further analysed, which means, a value of 21160. For these values, it is found an entrance length of 486 mm. This value is about 23 times the tube's diameter. So, a round number of 25 times the diameter was used for the tube length, i.e., 525 mm (see Figure 2.1).

2.1.2. Meshing

To snap the mesh to geometric features, such as corners in *stl* files, it was created a file, inside system directory, named *surfaceFeatureExtractDict*. This way, it is possible to extract features from the surfaces. It is asked from the software to extract lines that intersect two surfaces that make an angle less than 91º between them. Also keep edges with more than two connected faces. Open edges were not extracted. This process was made to all *stl* files as described. An example of the dictionary may be seen in Figure 2.2. Output *eMesh* files were created.

```
Art2D_wallL.stl
{
    // How to obtain raw features (extractFromFile || extractFromSurface)
    extractionMethod    extractFromSurface;

    extractFromSurfaceCoeffs
    {
        // Mark edges whose adjacent surface normals are at an angle less
        // than includedAngle as features
        // - 0  : selects no edges
        // - 180: selects all edges
        includedAngle   91;
    }

    subsetFeatures
    {
        // Keep nonManifold edges (edges with >2 connected faces)
        nonManifoldEdges       yes;

        // Keep open edges (edges with 1 connected face)
        openEdges       no;
    }


    // Write options

        // Write features to obj format for postprocessing
        writeObj               yes;
}
```

Figure 2.2. Example of code at *surfaceFeatureExtractDict*.

The next step consists on creating a base mesh. This is made using *blockMesh* utility. With it, a rectangular domain was created, fitting the geometry of all *stl* files. It was chosen a mesh with 280 blocks in the X direction, 200 in the Y direction and 1 in the Z direction. In *blockMeshDict*, front and back faces are set with empty condition, so that the problem is modelled as 2D. The other surfaces are set with patch condition. The *blockMeshDict* can be seen at Annex A.

Finally, *snappyHexMesh* utility was used to generate the mesh. The dictionary from multiphase, interFoam, ras, DTCHull tutorial was copied as a starting point. Also mesh quality controls were taken from the same tutorial. Only the changes made to original *snappyHexMeshDict* are described here.

The geometry must be indicated, referring to *stl* files created before. The name given to each patch is the same as the geometry file. Both walls were set with type wall. The inlet and the outlet were set with type patch. In features subsection, inside "castellatedMeshControls" section, were defined all *eMesh* files, with a null refinement level. Also, in subsection "refinementSurfaces" were set the surfaces, previously spoken, with a null refinement level. The reference point, one that must be inside the final meshed zone, is set to "(0 0 0)". This is the point in the centre of the entrance. Concluding, *castellatedMesh* and *snap* properties were set to "yes". No layers were added. The grid that resulted from this is represented at Figure 2.3.

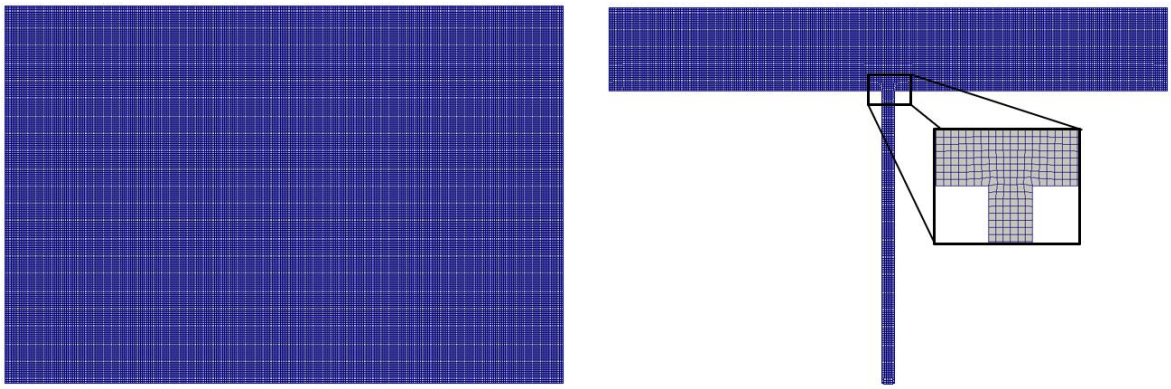

Figure 2.3. Mesh before and after executing *snappyHesMesh* utility.

2.1.3. Boundary conditions and constants

The boundary conditions are set inside the first "time" folder (*0*). They are summarised at Table 2.1. The patches *front* and *back* are set as empty, for all properties.

Table 2.1. Boundary and initialization conditions.

Property	Boundary	Type	Details
alpha.water	Left wall	zeroGradient	-
	Right wall	zeroGradient	-
	Inlet	fixedValue	value uniform 1
	Outlet	inletOutlet	inletValue uniform 0 value uniform 0
	Internal field	-	uniform 0
p_rgh	Left wall	zeroGradient	-
	Right wall	zeroGradient	-
	Inlet	zeroGradient	-
	Outlet	totalPressure	p0 uniform 0
	Internal field	-	uniform 0
U	Left wall	noSlip	-
	Right wall	noSlip	-
	Inlet	fixedValue	value uniform (0 V 0)
	Outlet	pressureInletOutletVelocity	value uniform (0 0 0)
	Internal field	-	uniform (0 0 0)

When “zeroGradient” is defined, the normal gradient of the field it is applied to, for example alpha.water (volumic fraction of water), is null. At the inlet, a fixed inlet velocity *V* is defined, for all time steps. Also, a uniform value of 1 for alpha.water, representing the liquid phase entering. The outlet is defined with inlet/outlet conditions. So, the property alpha.water may enter or exit the domain through that boundary. When it enters, it’s value is null. In Greenshields (2017), page U-142, it is suggested to combine “totalpressure” with “pressureInletOutletVelocity” for situations of inlet/outlet boundaries, where inlet conditions are not known. Velocity at walls is null. The property p_rgh is the subtraction of hydrostatic pressure to total pressure. The reference value of zero is set at the outlet.

The boundary conditions associated to turbulence modelling, which is addressed in Section 2.2, are summarised at the Table 2.2. The walls have the respective wall functions associated, to compensate high velocity gradients near them. Here, the outlet patch is also set with "inletOutlet" condition. For "nut" (turbulent viscosity), at the outlet, its value is calculated attending to other properties. The inlet condition is set to zeroGradient because there is no data about turbulence properties there.

Table 2.2. Boundary and initialization conditions related to turbulence.

Property	Boundary	Type	Details
k	Left wall	kqWallFunction	uniform 0.1
	Right wall	kqWallFunction	uniform 0.1
	Inlet	zeroGradient	-
	Outlet	inletOutlet	inletValue uniform 0 value uniform 0
	Internal field	-	uniform 0.1
epsilon	Left wall	epsilonWallFunction	uniform 0.1
	Right wall	epsilonWallFunction	uniform 0.1
	Inlet	zeroGradient	-
	Outlet	inletOutlet	inletValue uniform 0 value uniform 0
	Internal field	-	uniform 0.1
omega	Left wall	omegaWallFunction	uniform 2
	Right wall	omegaWallFunction	uniform 2
	Inlet	zeroGradient	-
	Outlet	inletOutlet	inletValue uniform 2 value uniform 2
	Internal field	-	uniform 2
nut	Left wall	nutWallFunction	uniform 0

	Right wall	nutWallFunction	uniform 0
	Inlet	zeroGradient	-
	Outlet	calculated	value uniform 0
	Internal field	-	uniform 0

Inside the *constant* directory some properties must be specified. There, the gravitational acceleration is set to -9.81 m/s^2, with the direction of Oy axis (see Figure 2.1). The phases must be specified. So, for water, it was set a kinematic viscosity of 1 mm^2/s and a density of 1000 kg/m^3. For air, a kinematic viscosity of 14.8 mm^2/s and a density of 1 kg/m^3 were defined. The surface tension is set to 0.07 kg/s^2. These values are the same found in the damBreak tutorial.

At the beginning of the simulation the tank is full of water. So, it is used the *setFields* utility. With it, a box, bounding all the walls, is created. All cells inside this box are assigned with the value 1 for alpha.water. The result is represented at Figure 2.4.

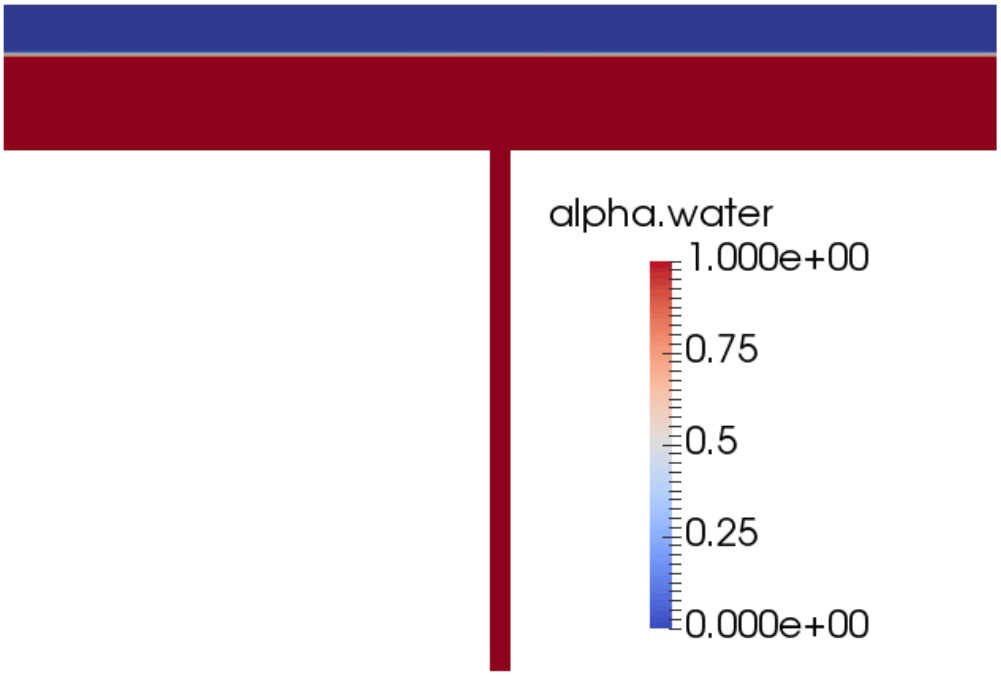

Figure 2.4. Alpha.water field after *setFields*.

The time step is set automatically by the software for a maximum Courant number of 0.95.

2.2. Turbulence models

For the setup previously explained and the mesh referred in Section 2.1.2, several RAS turbulence models were tested. This was made for two inlet velocities. The first one has a value of 0.62 m/s and creates a stationary regime. The second one, with a value of 0.782 m/s, represents the transition to an oscillatory regime, with a frequency of oscillation of 1.623 Hz (Espa and Frattini, 2002). For each velocity, it was analysed the occurrence or not of jet flapping, which results are shown in Table 2.3. If there is oscillation for the higher velocity, frequency is analysed visually, timing a certain number of oscillations. Time of simulation was initially set equal to 10 seconds.

Table 2.3. Jet oscillation results for several turbulence models.

Turbulence model	V = 0.620 m/s	V = 0.782 m/s
Laminar	Oscillatory	-
Standard k-ε	Stationary	Stationary
k-ω SST	Stationary	Oscillatory
Standard k-ω	Oscillatory	Oscillatory
k-ε realizable	Stationary	Oscillatory

Without any turbulence model, jet oscillated for the lower velocity, contrarily to the experimental observation of Espa and Frattini (2002). This is an indicator that a turbulence model is necessary.

Using a standard k-ε model a stationary regime was found for the lower velocity, as expected. This regime was also observed for second velocity, which resulted in the rejection of such model.

For k-ω SST, there is no oscillation for the lowest velocity. But, for the higher one, jet started to flap near the end of simulation time. Taking this into account, simulation time was increased to 50 seconds. The frequency of oscillation was calculated based on the 40.5 oscillations verified between the 19 and 50 seconds of simulation time, which corresponds to 1.306 Hz.

Near 50 seconds of simulation time, jet flapping initiation was visible using the standard k-ω turbulence model, for the lower velocity, as shown in Figure 2.5. Therefore, this model is also rejected.

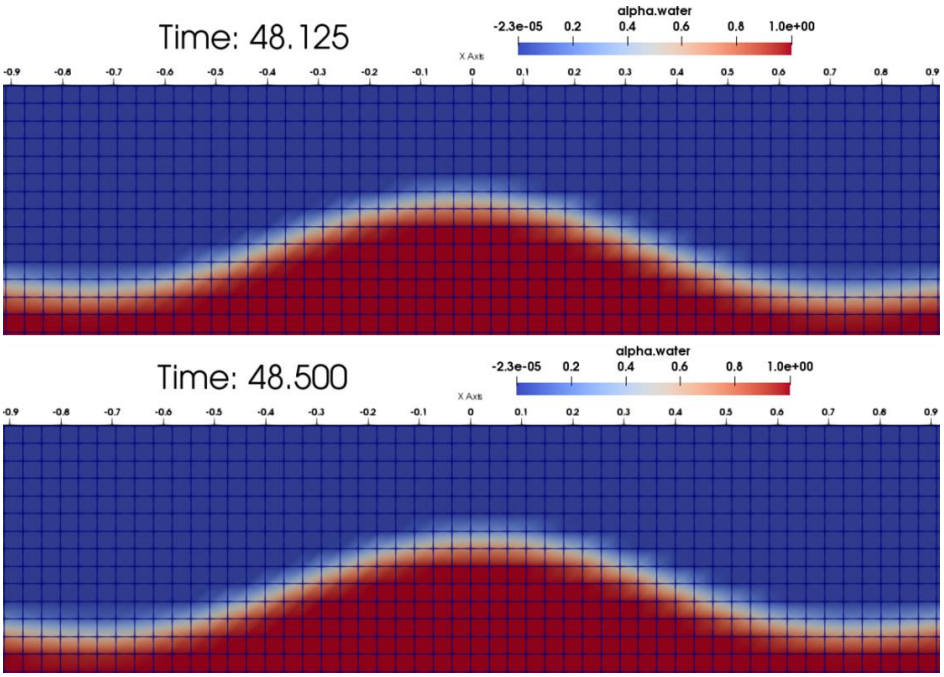

Figure 2.5. Detail for jet oscillation using standard k-ω model with V = 0.620 m/s.

Finally, the k-ε realizable model was also tested, giving identical results as k-ω SST model, in terms of oscillation. The frequency of oscillation was found to be 1.133 Hz, considering the 34 oscillation cycles between 20 to 50 seconds of simulation time.

As can be seen at Annex B, where screenshots are taken for the latest time step of each simulation for the lower velocity, the flow pattern inside the tank is very similar for all models. There is a jet impingement point, two recirculation cells at both sides of the jet and then the flow direction is almost horizontal. Only the standard k-ω gives a larger recirculation cell near the vertical walls of the tank. All the others are smaller compared to this model.

At Annex C are screenshots for the latest time step, related to the velocity of 0.782 m/s. There may be seen the lack of oscillation associated to standard k-ε model. All other images present a deflected jet, indicating an oscillating regime. Regarding the flow pattern, the same characteristics mentioned in the previous paragraph are visible too.

The previous conclusions were enough to choose k-ω SST turbulence model for future simulations, as it predicts a frequency closer to the experimental observation of 1.623 Hz, for an inlet velocity of 0.782 m/s.

2.3. Model height influence

Above the water surface there is air flowing, and for results from Section 2.2, the top boundary of the domain is close to the impingement point, as may be seen at Annex D. The influence of the height of the air domain above the water on its flow and frequency of oscillation is investigated.

To do this, the outlet geometry was modified to have a height of 50, 110 or 170 mm. The number of cells on Y direction had to be adapted, to keep the cell size. Values of this changes may be found on Table 2.4.

Table 2.4. Adaptation to number of cells at vertical direction.

Outlet height [mm]	Model total height [mm]	Number of cells at Oy direction	Cell height [mm]
50	673	200	3.365
110	733	218	3.362
170	793	236	3.360

Again, simulations were performed for two inlet velocities, 0.620 and 0.782 m/s, respectively. Values of alpha.water were sampled in two vertical lines, when the jet wasn't oscillating. So, for the lowest velocity (see Table 2.5), samples were taken at the end of the simulation, t=50 seconds. On the other hand, for a velocity of 0.782 m/s (Table 2.6), samples were taken at t=5 seconds of simulation (Annex D). The vertical lines were set for x equal to 0 and 0.4 metres, i.e., at the jet axis and at the line that intersects point P_2, visible at Figure 2.6. To analyse the height of water at those lines, samples were taken for every cell boundary that the line intersects. Then, a linear interpolation, between the first values above and under 0.5 of alpha.water, is done. The water height is relative to the tank bottom. The frequency was calculated considering the number of oscillations observed between 19 and 50 seconds of simulation time.

Table 2.5. Water height at sample lines for V=0.620 m/s.

Outlet height [mm]	Water depth (x=0 m) [mm]	Decrease	Water depth (x=0.4 m) [mm]	Decrease
50	130.99	-	114.91	-
110	130.02	0.74 %	113.85	0.92 %
170	129.23	0.61 %	113.44	0.36 %

Table 2.6. Water height at sample lines for V=0.782 m/s.

Outlet height [mm]	Water depth (x=0 m) [mm]	Decrease	Water depth (x=0.4 m) [mm]	Decrease	Frequency of oscillation [Hz]	Increase
50	143.62	-	117.46	-	1.306	-
110	142.08	1.07 %	115.73	1.47 %	1.323	1.30 %
170	142.26	-0.13 %	115.47	0.22 %	1.339	1.21 %

The increase of the domains height origins a descendent air flow. This flow interacts with the water free surface, slightly decreasing water depth for all situations. Only for V=0.782 m/s, and an outlet height of 170 mm, water depth increases slightly at the impingement point. Nevertheless, the frequency also changes, but only a little, having the consecutive increases of its value shown at Table 2.6. So, it is concluded that the outlet height has little effect on the oscillation pattern. A third velocity, equal to 1.008 m/s, is studied in Espa and Frattini (2002), which is a higher velocity than the two previously mentioned. So, to make sure that the water does not touch the upper boundary, the outlet height of 170 mm was chosen.

2.4. Mesh refinement study

A mesh refinement study was performed, considering an inlet velocity of 1.008 m/s. Meshes were only modified in *blockMeshDict*. To analyse frequency of oscillation, the same method previously mentioned was used. Also, a power spectrum analysis (psd) was

made for every mesh, using software Microsoft Excel. This analysis was made probing horizontal and vertical velocities at two points, of coordinates (0.015 m; 0.070 m; 0.000 m) for P_1 and (0.400 m; 0.070 m; 0.000 m) for P_2, as Espa and Frattini (2002) did on their work (see Figure 2.6). Probing was set to begin after 15 seconds of simulation, when the flow is already oscillatory, writing values every 0.008 seconds. Results of psd analysis may be seen on Annex E.

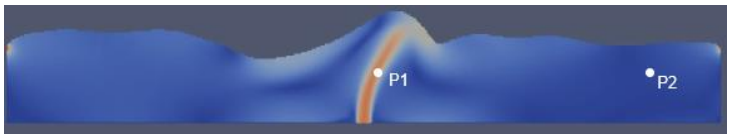

Figure 2.6. Location of points P_1 and P_2.

Table 2.7. Frequency of oscillation for several meshes.

Name	Mesh	psd frequency [Hz]	Error to experimental [%]	Error to finest mesh [%]	Visual frequency [Hz]
Exper.	-	1.416	-	-	1.416
ref_1	140x118	no oscillation	-	-	-
ref_2	280x236	1.393	1.624	11.619	1.381
ref_3	420x354	1.357	4.167	8.734	1.353
ref_4	560x472	1.343	5.155	7.612	1.329
ref_5	700x590	1.297	8.440	3.926	1.304
ref_6	840x708	1.277	9.818	2.324	1.280
ref_7	980x826	1.248	11.864	0.000	1.240

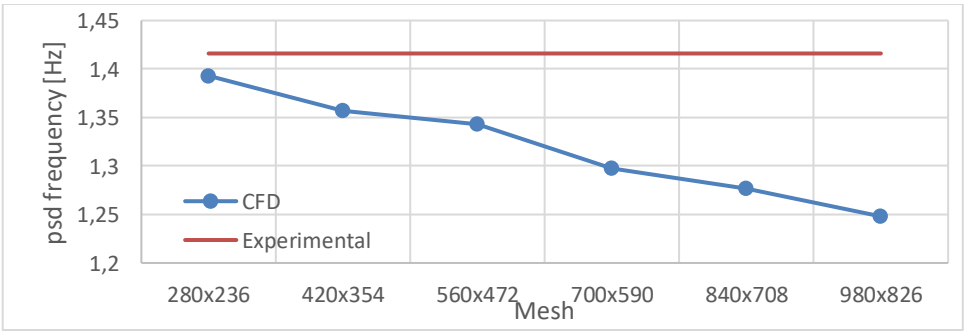

Figure 2.7. Frequency of oscillation of the jet vs mesh.

Comparing the frequency values given by the psd analysis and visual inspection, very close values, for all grids, are observed. This is a good indicator that psd has been done correctly. Also, the visual analysis of the frequency is accompanied by bigger errors because the observer of the number of oscillations can't find the jet in the exact same state as in the beginning of the timing, due to a write interval of 0.2 seconds, while the psd analysis uses values written every 0.008 seconds, as mentioned.

The mesh refinement study resulted in an erratic behaviour regarding frequency of oscillation. In fact, the frequency never stabilised, always increasing its discrepancy relatively to the experimental value, as shown in Figure 2.7. Also, the frequency value goes down as the mesh is refined, as indicated in Table 2.7. At a certain point, the mesh becomes too heavy to consider a future 3D situation.

2.5. Convergence criteria modification

At the *fvSolution* file, inside the *system* directory, several convergence criteria values were modified, one by one, as shown at Table 2.8, trying to approximate the frequency of oscillation to its experimental value, for a velocity of 1.008 m/s, as in previous section. So, several iterations were made, using an intermediate mesh of 420x354. Again, psd analysis were performed and, for the simulation, an Intel® Core™ i7-7700HQ CPU at 2.80GHz with 4 cores was used. The results for psd may be found on Annex F.

Table 2.8. Convergence criteria modifications.

Name	pcorr tol.	U tol.	k tol.	ω tol.	psd frequency [Hz]	Error to experimental [%]	Clock time [hh:mm:ss]
Exper.	-	-	-	-	1.416	-	-
tol_1	10^{-5}	10^{-6}	10^{-6}	10^{-6}	1.357	4.167	01:22:02
tol_2	10^{-8}	10^{-6}	10^{-6}	10^{-6}	1.387	2.048	03:01:25
tol_3	10^{-8}	10^{-8}	10^{-6}	10^{-6}	1.387	2.048	01:21:13
tol_4	10^{-8}	10^{-6}	10^{-8}	10^{-6}	1.397	1.342	03:20:44
tol_5	10^{-8}	10^{-6}	10^{-8}	10^{-8}	1.396	1.412	02:03:41
tol_6	10^{-8}	10^{-8}	10^{-8}	10^{-8}	1.396	1.412	02:02:54

After decreasing the tolerance for pressure correction (pcorr), the error to the experimental halved, although, calculation time more than doubled. Then, for the case tol_3, the velocity tolerance was also dropped. This made no changes on frequency, but the clock time reduced to half. Despite this, that tolerance was reset, and the k tolerance was decreased. Relatively to the case tol_2, the clock time slightly increased but the frequency error deduced also. For tol_5, comparatively to tol_4, the ω tolerance is changed. This almost did not influence the frequency of oscillation but reduced clock time to about 2 hours. To reduce calculation time even more, the velocity tolerance was reduced again. Similarly, to the previous reduction of this value, the frequency did not change. The clock time was not reduced much.

From this study, the frequency error was downsized from 4.167 % to 1.412 % only increasing the clock time on about 40 minutes. So, the convergence criteria according to the tol_5 case were chosen for further study.

2.6. Simulation vs experimental

Using results from the previous case, further post processing was done to better compare results with the experimental data.

At Figure 2.8 free surface is visualized. Time steps from the simulation were chosen to best adapt to the original images from Espa and Frattini (2002), as write interval was set to 0.1 seconds of simulation. A threshold of alpha.water values, between 0.05 and 0.95, was sufficient to get the free surface shape. This image was then overlapped with the one from Espa and Frattini (2002).

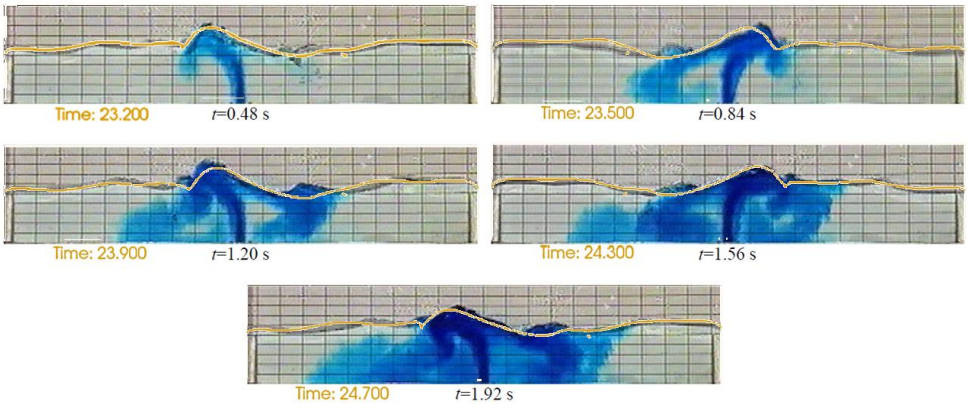

Figure 2.8. Free surface visualization for several time steps, for simulation (yellow) and experimental data (Espa and Frattini, 2002).

The computational free surface shape has the same behaviour as the experimental one. Only immediately behind the impingement point there is a wave on the experimental results, that does not appear at the OpenFOAM® results.

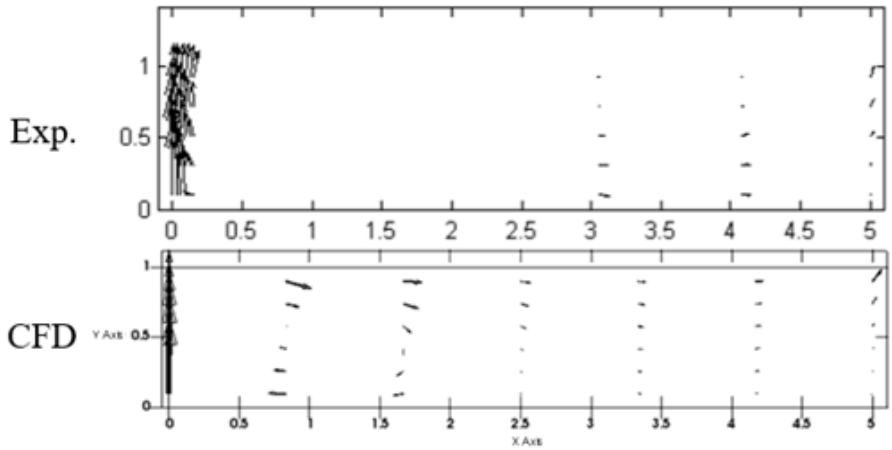

Figure 2.9. Time averaged velocity field for experimental (Espa and Frattini, 2002) and CFD.

Time averaged fields for velocity and turbulent kinetic energy were calculated at every cell. Inside OpenFOAM®, this is done inside *controlDict* with the function "fieldAverage". This function calculates a new mean value at every time step. It was only activated after 15 seconds.

Figure 2.9 shows the time averaged velocity field. The coordinates are normalized by the spillways height (98 mm). From the experimental study, it is possible to see a deceleration of the fluid at the jet axis. The same was predicted by CFD. For a normalized horizontal coordinate superior to 3, a slight difference appears. Experimental results shown higher velocities near the bottom. Contrary to this, simulation gives more homogeneous velocity vectors, being velocity higher near the free surface. Again, recirculation cells at each side of the jet appear at the simulation results. The same happens experimentally, as can be seen on Figure 2.8.

Espa and Frattini (2002) normalize turbulent kinetic energy, and power spectrum density, to half of the square of the inlet velocity, calling it *tke* and *psd*, respectively. Higher values of *tke* appear near the jet and closer to the free surface. In the outlet zone lower values were observed.

From CFD (see Figure 2.10), higher values of *tke* can be seen at the side of the jet, spreading horizontally when the jet direction is followed. Contrary to the experimental results, near the free surface at impingement point, *tke* does not take values much higher than those near the bottom. Closer to the outlet, lower values of tke appear. On the zone where

there are no experimental results, high values are predicted where the flow, according to Figure 2.9, turns its direction into the jet again.

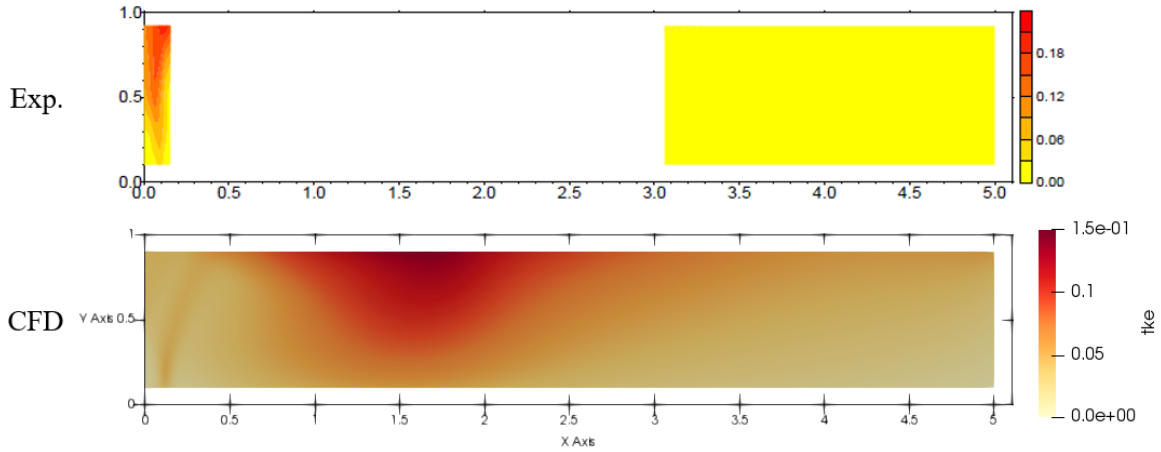

Figure 2.10. Time averaged and normalized turbulent kinetic energy field for experimental (Espa and Frattini, 2002) and CFD.

Espa and Frattini (2002) found, on their *psd* charts, Figure 2.11, that, for both points, two frequencies are evident. Also, the measured frequency, obtained timing one hundred oscillations, is concordant to the one from psd analysis. The peak for the vertical velocity is higher than for the horizontal one at P_1. For P_2 the opposite happens. Also, *psd* peak values are lower for P_2 than for P_1.

The latest considerations can be made to CFD results, as shown at Figure 2.12.

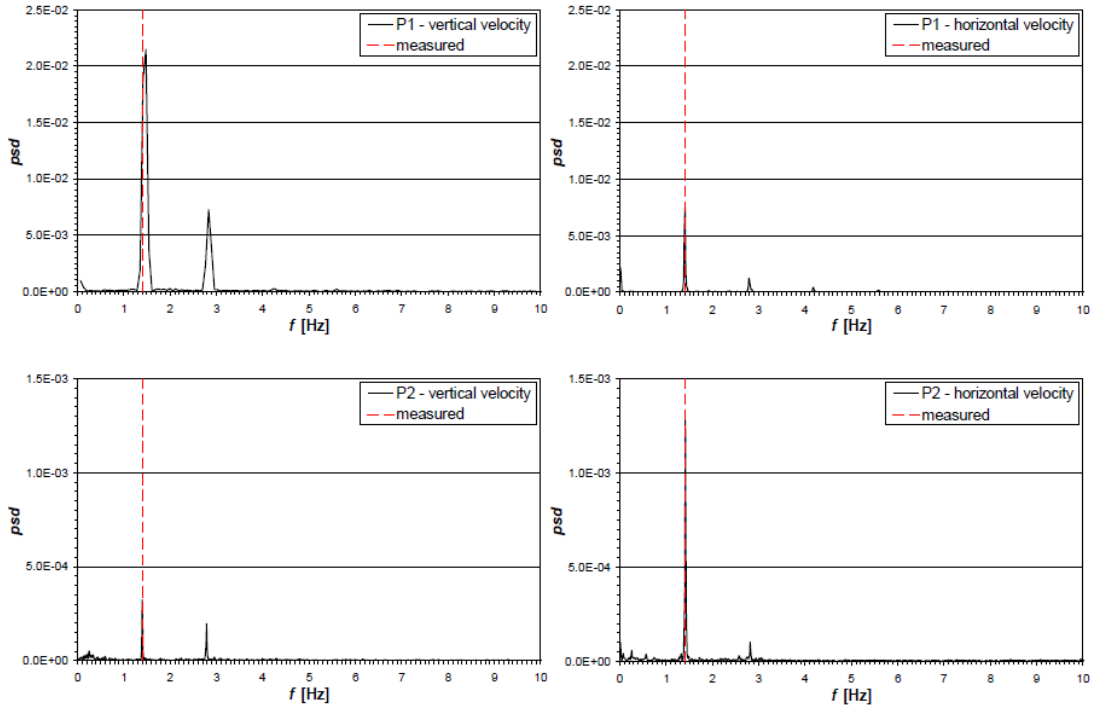

Figure 2.11. *psd* charts by Espa and Frattini (2002).

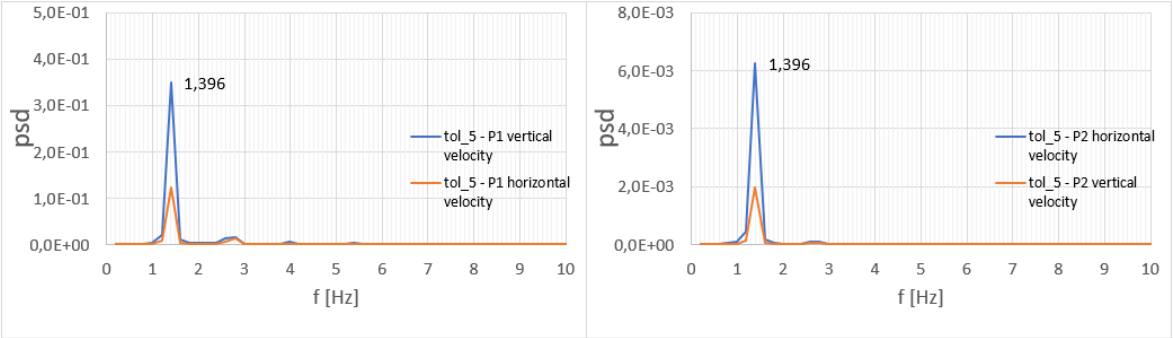

Figure 2.12. *psd* charts from CFD.

3. DEVELOPMENT

3.1. Plate in 2D case

3.1.1. Plate geometry

To eliminate the harmful oscillation of the central jet, a plate was introduced in the tank. This plate ("plate 1") is 2 mm thick and has a length of 4 times the tube diameter. It is placed at one diameter above the bottom. All mesh cells closer than half diameter of the tube are refined with level 2 (see Figure 3.1), relatively to the mesh prescribed in the *blockMeshDict*.

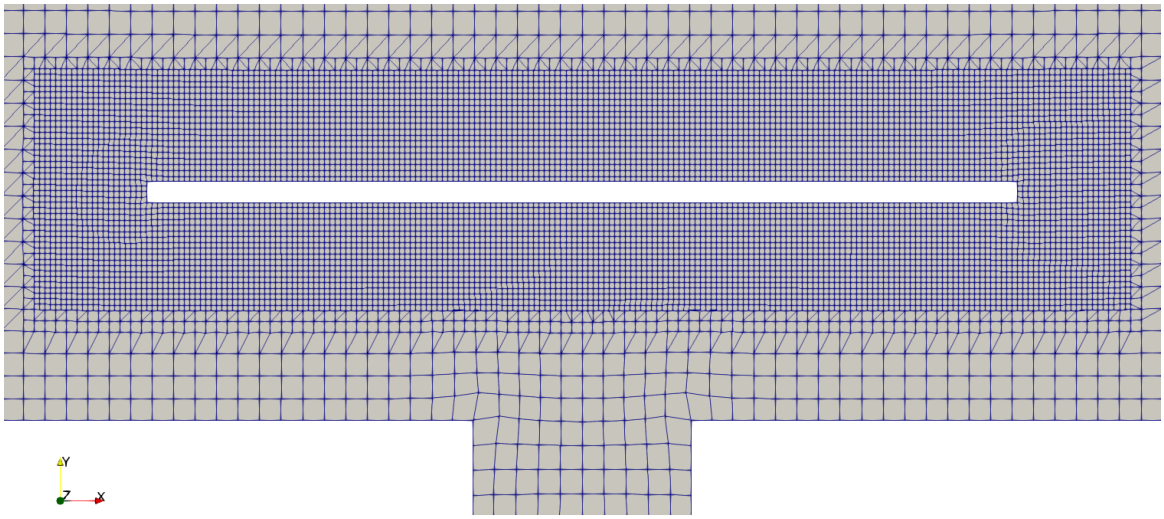

Figure 3.1. Mesh around plate 1.

The jet, when it hits the plate, divides into two horizontal jets, as shown in Figure 3.2. Then, the fluid flows near the bottom of the tank, exiting at the weirs. Two large recirculation cells appear on both sides of the tank, even though the free surface does not oscillate. These are not convenient because the dark spots, dropping from the gloves onto the tank, will not be able to flow out the tank. These cells create a depression at the centre of the tank.

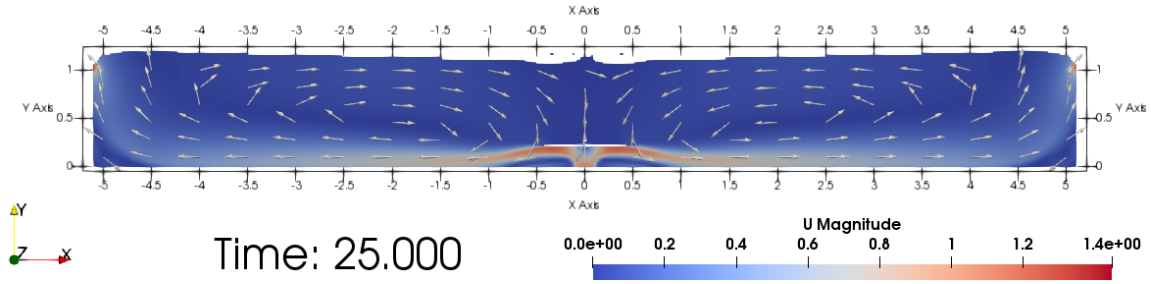

Figure 3.2. Velocity field and free surface shape for plate 1.

To solve the previous problems, holes with 5 millimetres of diameter were drilled in the plate ("plate 2"), illustrated in Figure 3.3. The distance between the closest points of two consecutive holes is 10 millimetres. The mesh refinement is the same as in the "plate 1" case.

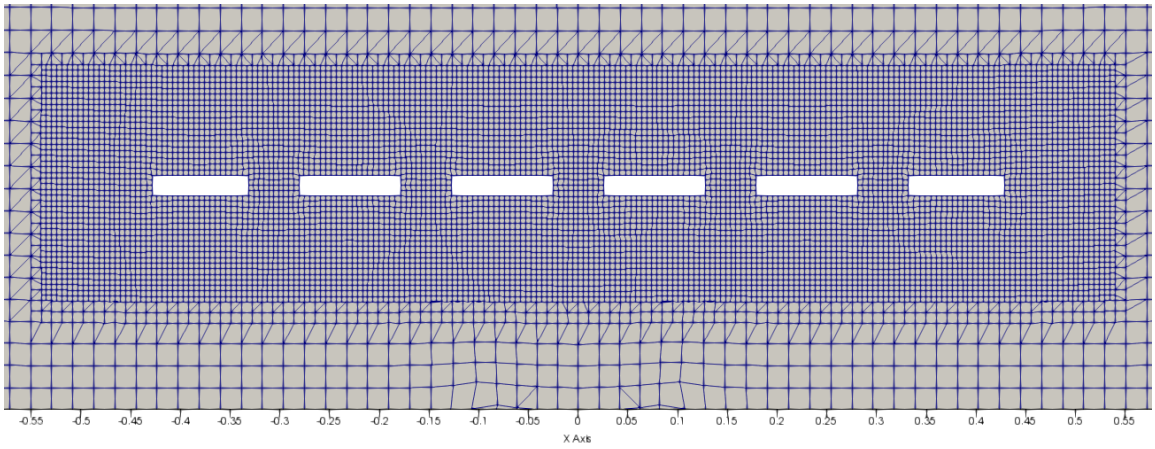

Figure 3.3. Mesh around plate 2.

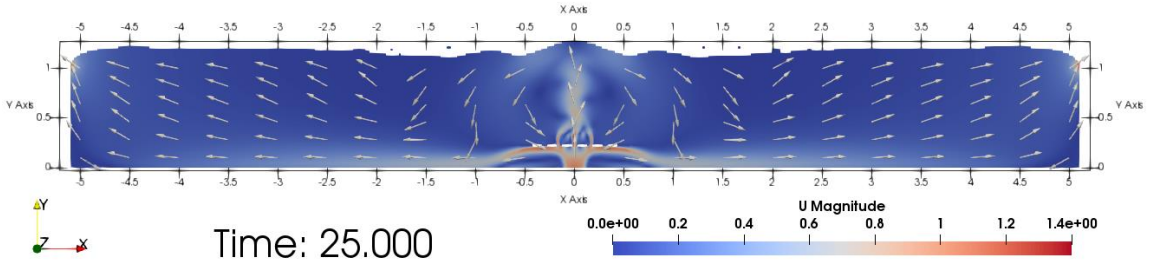

Figure 3.4. Velocity field and free surface shape for plate 2.

For "plate" 2 geometry, a non-oscillating swallow is formed on the free surface. The introduction of holes helped eliminating the recirculation cells, as the fluid near the free surface is directed to the weirs. Some inlet flow still hits the plate and deflects to the sides, following a trajectory near the bottom of the tank, as shown in Figure 3.4.

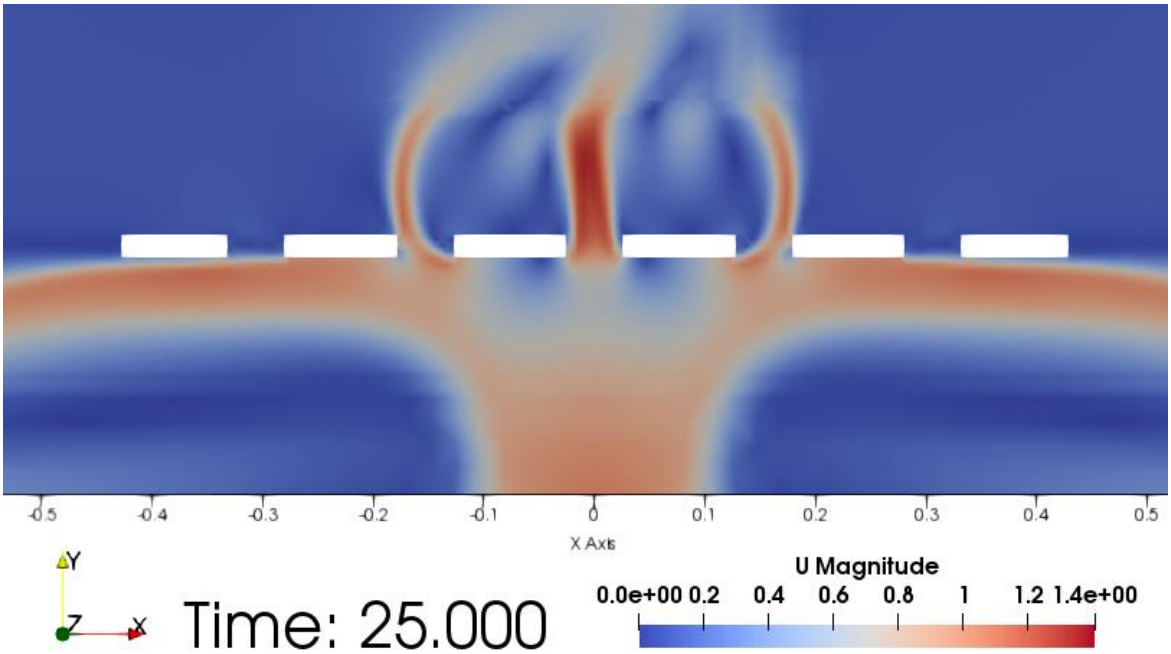

Figure 3.5. Detail of flow near plate 2.

Near the plate, as Figure 3.5 shows, the centre jet is stronger. At the next holes, two weaker and curved jets are also formed. These last connect to the central jet, oscillating. This oscillation dissipates near free surface, not interfering with it. At the rest of the holes, no jets are formed.

In a third plate ("plate 3"), the holes diameter was set equal to 2 millimetres, and its quantity increased to 11, decreasing the distance between consecutive holes to 5 millimetres, as visible in Figure 3.6.

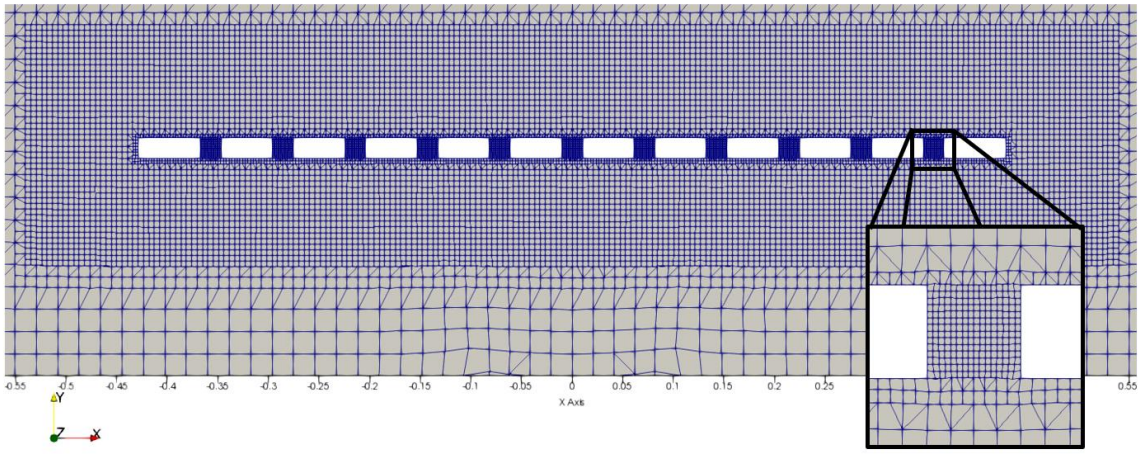

Figure 3.6. Mesh around plate 3.

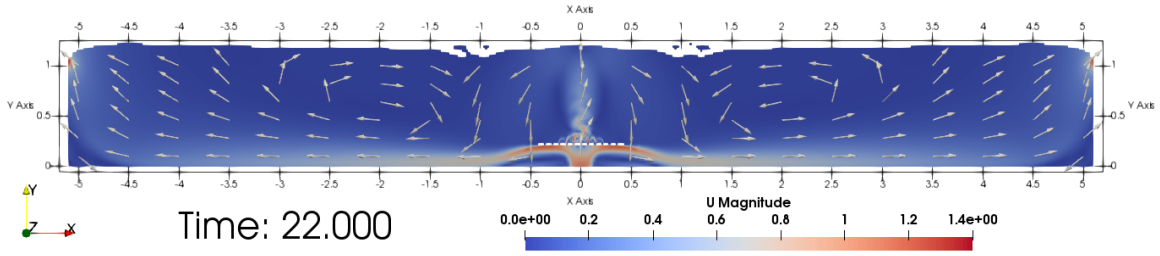

Figure 3.7. Velocity field and free surface shape for plate 3.

For this geometry free surface is flatter than for "plate 2". It also does not oscillate. Despite this improvement, recirculation cells near the free surface appear again, at each side of the tank (see Figure 3.7). The fluid that doesn't pass the holes is deflected, following a path near the bottom of the tank, as previously observed.

The flow near the plate has the same characteristics of the "plate 2" case. Centre hole's jet is stronger. When getting away from the centre, the jets get weaker. At the last two holes, at each end of the plate, no jets are formed, as visible in Figure 3.8. All jets curve and stick to the central one, creating an oscillatory pattern above the plate, that dissipates before reaching the free surface.

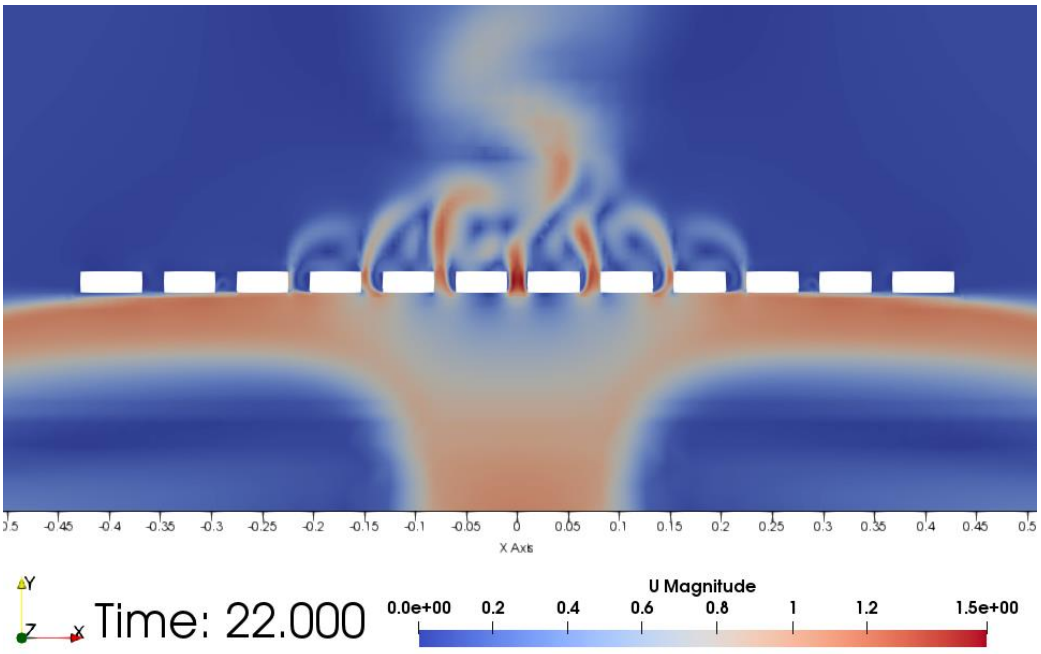

Figure 3.8. Detail of flow near plate 3.

Attending to these conclusions, plate might be narrowed. Also, trying to separate the jets from each other, inclination was given to the holes. This way, "plate 4" was created, as depicted in Figure 3.9.

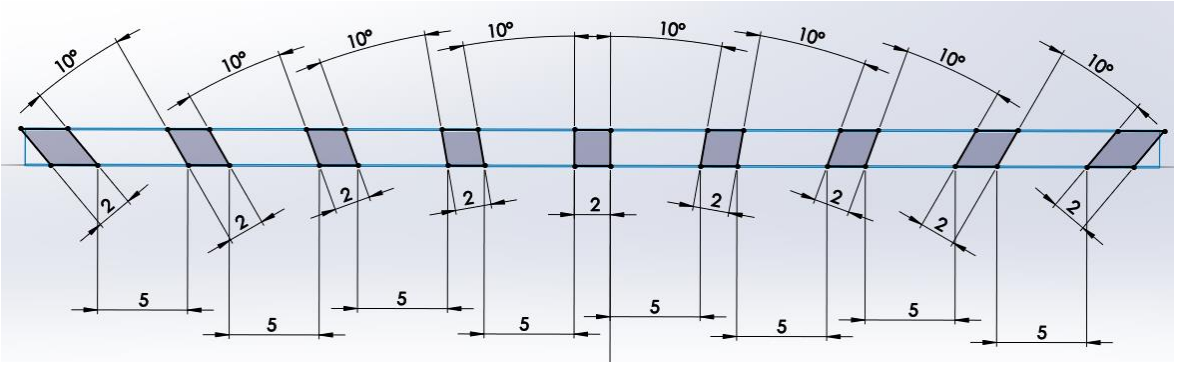

Figure 3.9. Geometry of plate 4 (dimensions in millimetres).

As Figure 3.9 shows, the 2 millimetres holes, spaced of 5 millimetres were kept. Now there are only 9 holes, as the plate length was downsized to 3 times the tube diameter. Each hole is rotated 10º relative to the previous one. Mesh refinement is the same as for "plate 3" (see Figure 3.10).

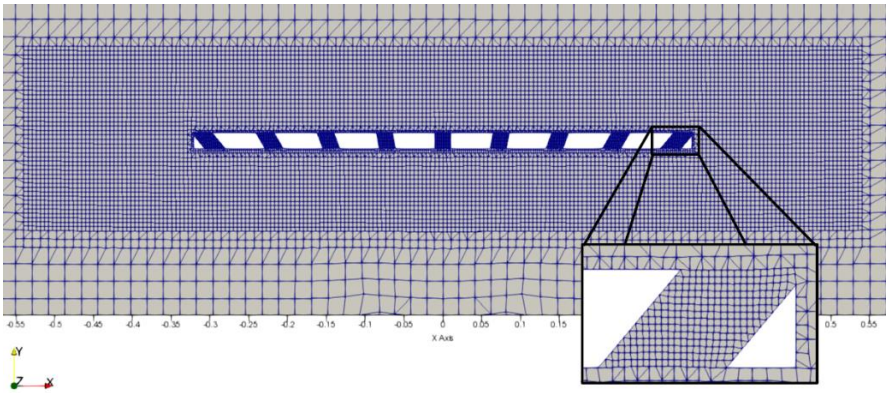

Figure 3.10. Mesh around plate 4.

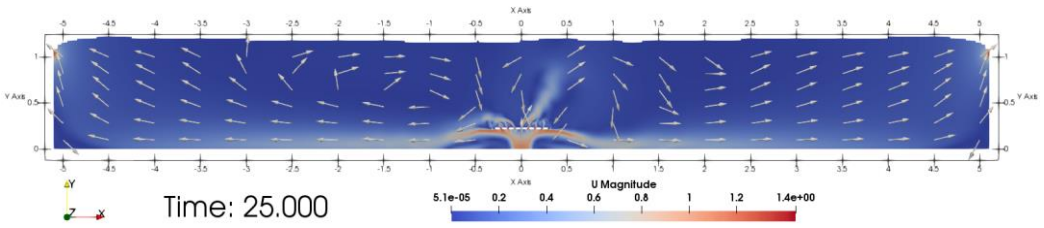

Figure 3.11. Velocity field and free surface shape for plate 4.

For this geometry of "plate 4", the free surface is flatter and doesn't oscillate. On the left side a low velocity recirculation zone appears, being the impingement point located slightly to the right, as shown in Figure 3.11. The inclination of the holes helped detaching some of the jets. In fact, Figure 3.12 shows that the jets from the right, and the central one, stick together. The same happens to the left ones. The asymmetry of the flow

begins around 0.6 seconds of simulation, as shown at Annex G, as the jet starts its natural oscillation. When it tumbles to one of the sides, immediately attaches to the jets at that side. The remaining flow is deflected and directed through the bottom of the tank.

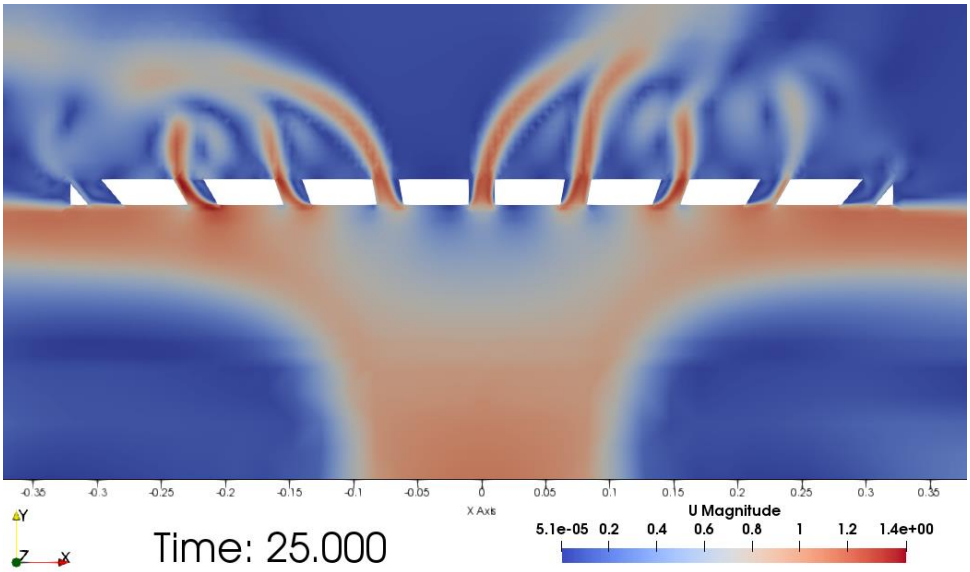

Figure 3.12. Detail of flow near plate 4.

3.1.1. Plate distance to bottom

With the last plate geometry (i.e., "plate 4"), it was tested if the plate distance to the bottom of the tank would change the flow.

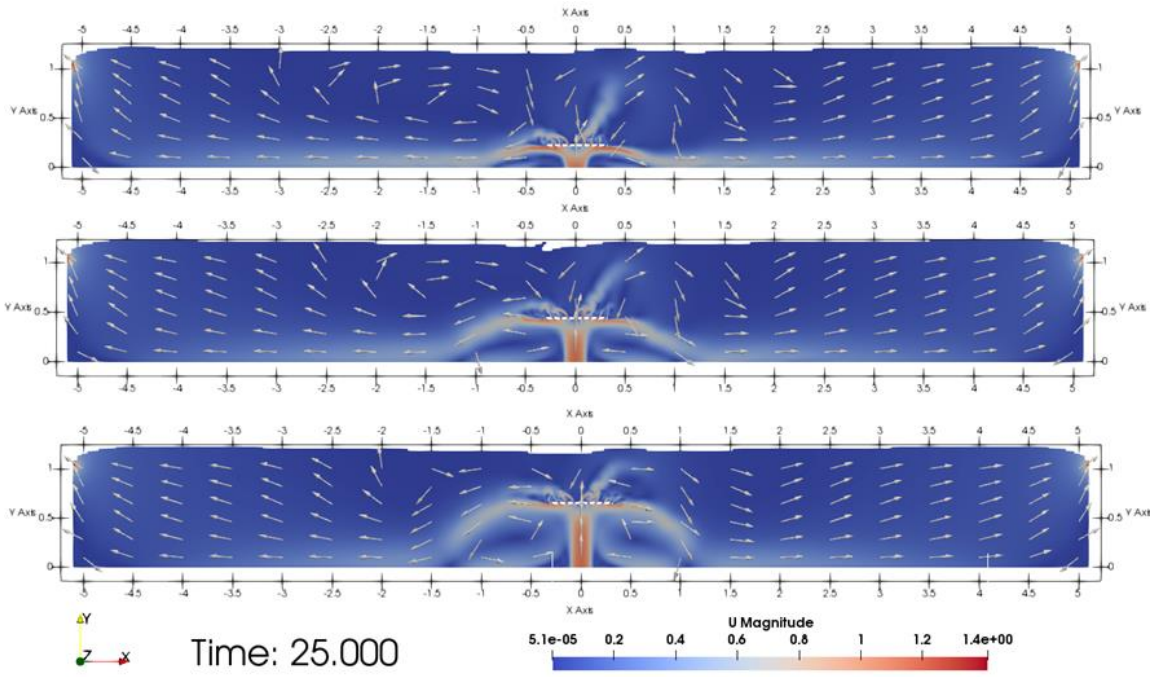

Figure 3.13. Velocity field for several plate distances to bottom.

The distance of the plate to the bottom was varied assuming values of 1, 2 and 3 times the diameter of the inlet tube. Figure 3.13 shows that the free surface shape does not change much. The central secondary jet is always deflected to one of the sides, for the reasons mentioned before. But, as the distance is increased, the velocity near the bottom of the tank is diminished. This is compensated by the presence of larger recirculation zones, of higher velocity, located on each side of the main jet. Near the outlets, no big changes are noticed. The recirculation bubble, present near the free surface at the left side of the tank, is shrunk as plate distance to the bottom increases.

As free surface doesn't change its shape considerably, internal flow is similar and the recirculation cell near the free surface is almost eliminated, a higher distance of the plate to the bottom of the tank has a positive impact on the overall flow.

3.2. Three-dimensional simulation

3.2.1. From 2D to 3D

As the real tanks represent a 3D case, a new simulation was set to observe the differences between the two-dimensional simulation and a three-dimensional one. So, a rectangular tank with a cylindric tube was designed. The boundaries of the domain are presented in Figure 3.14, where green surfaces are the outlet and grey ones are the walls. Inlet is not shown but consists of a circle positioned in the beginning of the entrance tube.

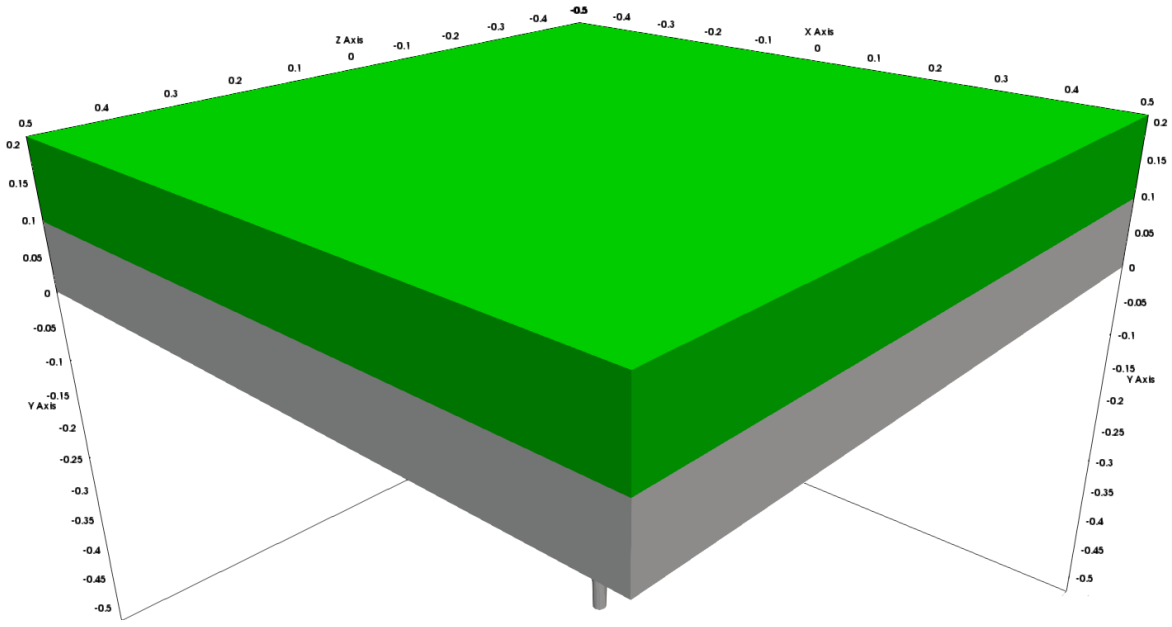

Figure 3.14. Geometry for 3D case (dimensions in m) based on the article by Espa and Frattini (2002).

A mesh like the one used before (Section 2.4) was attempted (420x354x420). With this mesh the software couldn't finish *blockMesh*, as the computer used hadn't enough memory to write 62 445 600 cells. So, a coarser mesh with 18 502 400 cells (280x236x280, like simulation "ref_2" from Section 2.4) was used. This mesh has, approximately, 3.57 mm cubic cells. To compare the results, a 2D simulation with this mesh, but with the convergence criteria used in Section 2.6, was also performed. All the other parameters are the same as the ones used in Section 2.6.

An overview of the free surface shape may be seen in Figure 3.15. A swallow appears in the centre of the tank, followed by a depression.

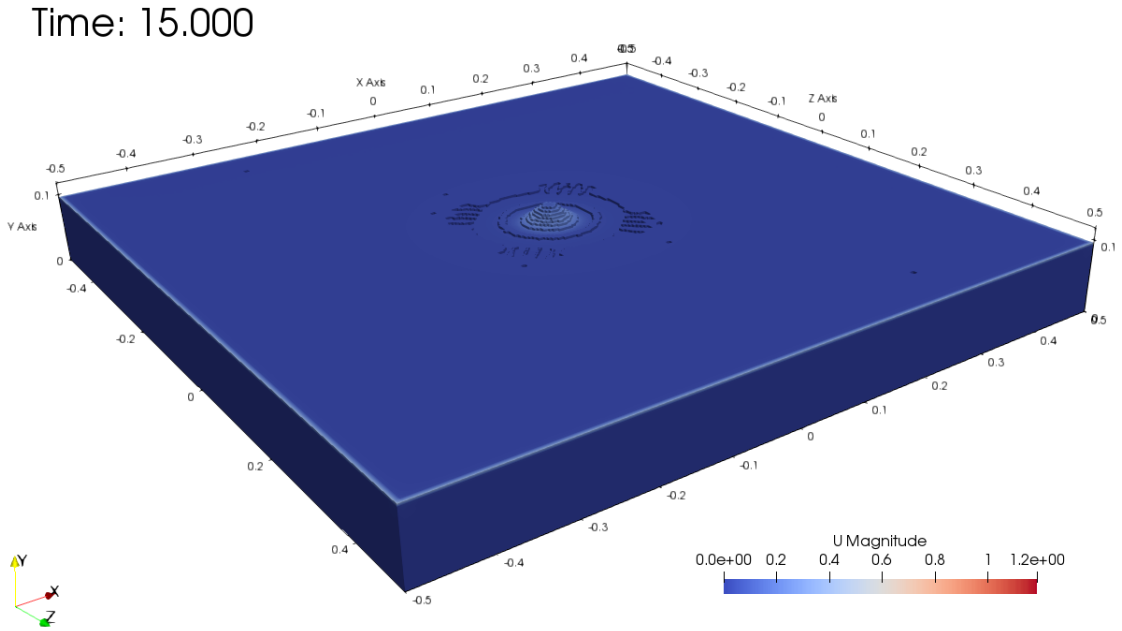

Figure 3.15. Free surface shape (dimensions in m).

For this case no oscillation was observed, as the instabilities that start and grow the jet oscillation are not strong enough. So, the loop mechanism observed in a plane jet does not apply to this 3D case.

At the region between the jet and the walls, velocities are much lower in the 3D case, as seen in Figure 3.16. The absence of waves, that provide higher velocities near free surface, and the increased domain volume, to be fed by the jet, are two reasons for this behaviour.

The recirculation cells at each side of the jet are much smaller in size, relatively to the 2D case presented.

At the free surface, the liquid flows radially, with its velocity decreasing like an exponential source flow. Attending to this reason, in Figure 3.17 darker spots appear near the corners of the tank, indicating zones of low velocity.

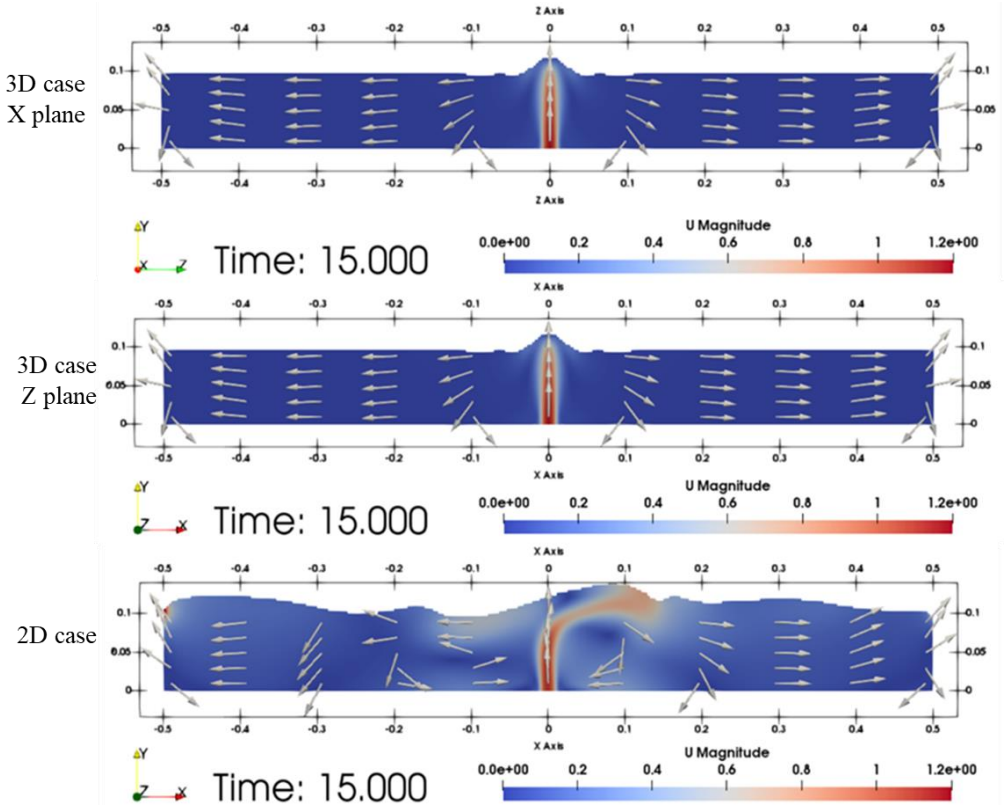

Figure 3.16. Velocity field, at planes that intersect origin point, for 3D and 2D cases (dimensions in m).

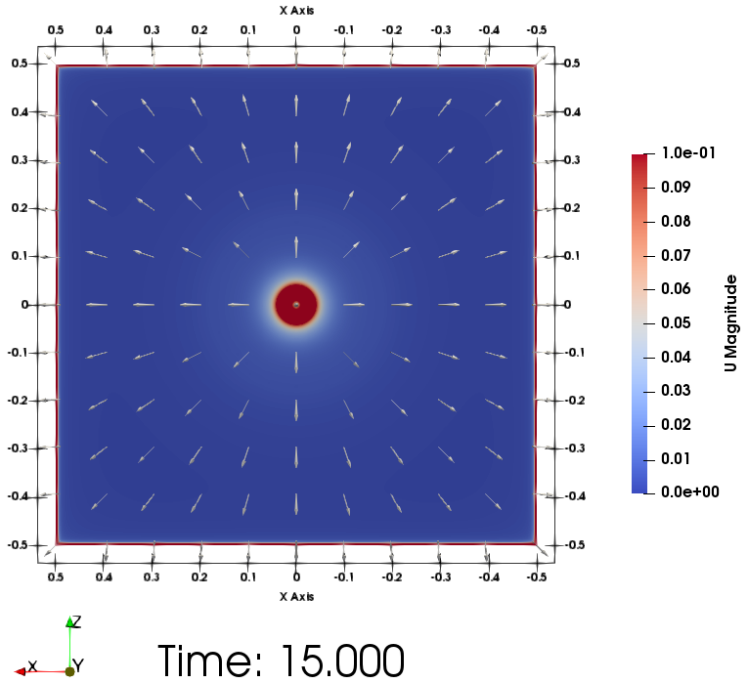

Figure 3.17. Velocity field at free surface for 3D case (dimensions in m).

3.2.2. LP2 tank

3.2.2.1. Case setup

To perform simulations of this section, the tank of the production line number 2 of Ansell factory (tank LP2) was chosen. As no data about its geometry was available, the tank was drawn using SOLIDWORKS®. Some images of this tank and pump's rotor geometry may be found at Annex H and Annex I.

The flow is induced by a centrifugal pump, at the lowest point, in height, of the tank. There, the rubber passes through a tube with 100 millimetres of diameter, entering in an inner tank, where the gloves are immersed. The rubber exits at spillways located on the laterals of the internal tank, being, under the effect of gravity, directed to the pump again.

Only some faces of the inner tank and the tube were considered for simulations. A *stl* file for the outlet, as in the previous cases, was created. The several geometries, and its dimensions, may be accessed at Annex J to Annex M.

Relatively to Figure 3.18, in red (tube), grey (bottom) and green (wall) are surfaces associated to wall boundary condition. The inlet patch appears in blue and the outlet in yellow. All the boundary conditions in these are the same, respectively, to the ones used in Section 2.1.3.

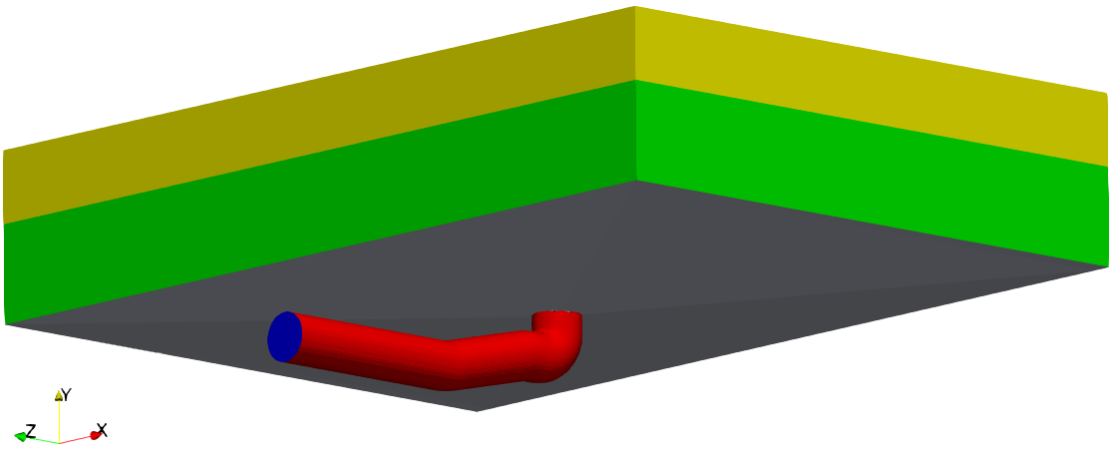

Figure 3.18. Surfaces used for simulations on LP2 tank.

The properties of the rubber are different from the ones used before (water properties). Its kinematic viscosity is of 199.8 mm^2/s, density of 1001 kg/m^3 and surface tension of 0.0395 kg/s^2.

Concerning the mesh, OpenFOAM® crashed for a cell size of 3.57 mm. So, the mesh was, once again, coarse to 6 mm cubic cells which, after running the *snappyHexMesh* utility, resulted in a total number of about 4 million cells.

3.2.2.2. Inlet flow rate

The flow rate was calculated using equation (3.1), for rectangular weirs (Mata-Lima et al. 2008),

$$Q = \frac{2}{3} \times C_d \times S \times H \times \sqrt{2gH}. \quad (3.1)$$

where Q is the volumetric flow rate, C_d the flow coefficient that depends on the weir shape, S the perimeter of the weir, H the height of fluid above the weir and g the gravitational acceleration (9.81 m/s^2).

C_d is assumed equal to 0.6, as in Espa and Frattini (2002). S and the height of the weir, relatively to the bottom, using the CAD designs of the tank, are 6.2 metres and 0.2 metres, approximately (Annex N and Annex O).

The height of the free surface, relatively to the tank's bottom, was measured with round wood sticks with 5 millimetres of diameter. The measures were taken 100 millimetres away from the weir. Five samples were taken, being the results shown at Table 3.1.

Table 3.1. Measures of free surface height to the bottom.

Sample number	Height of the free surface [m]
1	0.2090
2	0.2080
3	0.2075
4	0.2060
5	0.2070

The average value is 0.2075 metres. Then, the value of H is 8.19 millimetres. The corresponding volumetric flow rate is 8.19 l/s.

Dividing the volumetric flow rate by the area of the cross section of the tube (100 millimetres of diameter), an average velocity of 0.26 m/s is achieved, corresponding a Reynolds number of 130.

3.2.2.3. LP2 results

The picture shown in Figure 3.19 corresponds to the conditions described in Section 3.2.2. A small swallow, dislocated from the centre of the tank, is visible. Also, darker zones (originated from dried rubber dripping from the hanging gloves) appear in the free surface, near two of the corners, on the opposite side of the tank. From observations at the local, those zones have low velocities, preventing the dark spots to flow out of the tank. Between these dark zones, there is a path where no spots are visible. This is an indicator that this zone has higher velocity with a trajectory from the centre to the walls.

Figure 3.19. Free surface on LP2 tank.

From the simulation done of the present case, which results are shown for a simulation time of 15 seconds, a similar image was foreseen (Figure 3.20) for a comparison with Figure 3.19. A small swallow also appears, displaced to the front. Relatively to darker spots, velocity is lower in the middle and not at the corners, as observed in the real flow.

Attending to Annex P, velocity at the free surface is higher for negative Z coordinates because the jet is projected in that direction. A stagnation point appears near the centre of the tank. The jet, after impinging the free surface, is orientated mainly for negative Z direction. Nevertheless, it is also projected to positive Z direction, with lower velocity,

and to both directions of X coordinate, symmetrically, being deflected to positive side of coordinate Z. Top velocities appear near the weirs.

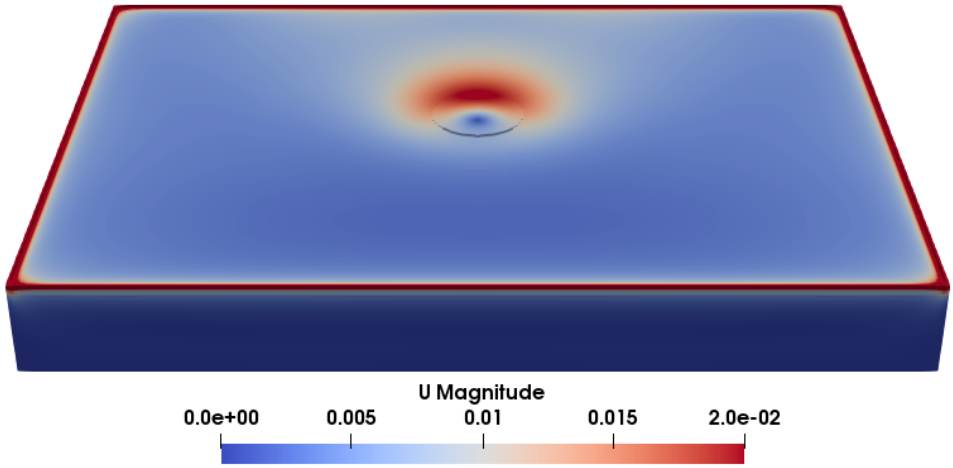

Figure 3.20. Free surface on LP2 tank's simulation.

At middle height of the tank, and also near the bottom, the same pattern is visible, i.e., a deflection of the jet toward negative Z direction. The jet is also diffused to the sides, being deflected to positive Z direction (see Annex Q and Annex R).

A slice tangent to the tube axis is shown in Figure 3.21. It is visible that the vertical part of the tube is not long enough to get a perfect vertical jet. In fact, the flow that comes from the inlet tube is deflected upwards but maintains a horizontal component. This justifies the location of the swallow, that is dislocated from the centre of the tank in the direction of the jet.

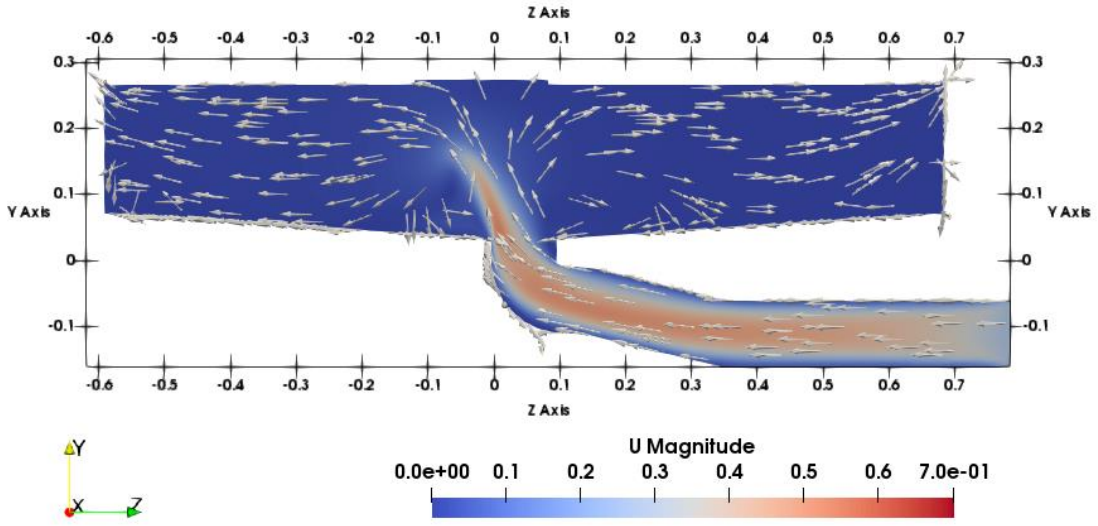

Figure 3.21. Direction of the flow through the tube (dimensions in m).

3.2.3. Deflector incorporation

3.2.3.1. Deflector incorporation in LP2 tank

The deflectors used at Section 3.1.1 were all plates. That flat geometry always resulted in the attachment of several secondary jets. For this LP2 case, aiming to solve such problem, a different geometry was used. So, it was designed a semi-sphere with a set of holes around it, as shown at Annex S.

An identical mesh, as the one used in Section 3.2.2, was used but, near the deflector, it is necessary a finer refinement. So, a box surrounding the semi-sphere, with a refinement level of 1 was applied. This box surrounds, and exceeds, the deflector, to the sides and top, 0.5 times the inlet tube diameter. Cells intersected by the deflector were set with a refinement level of 3, as observed in Figure 3.22.

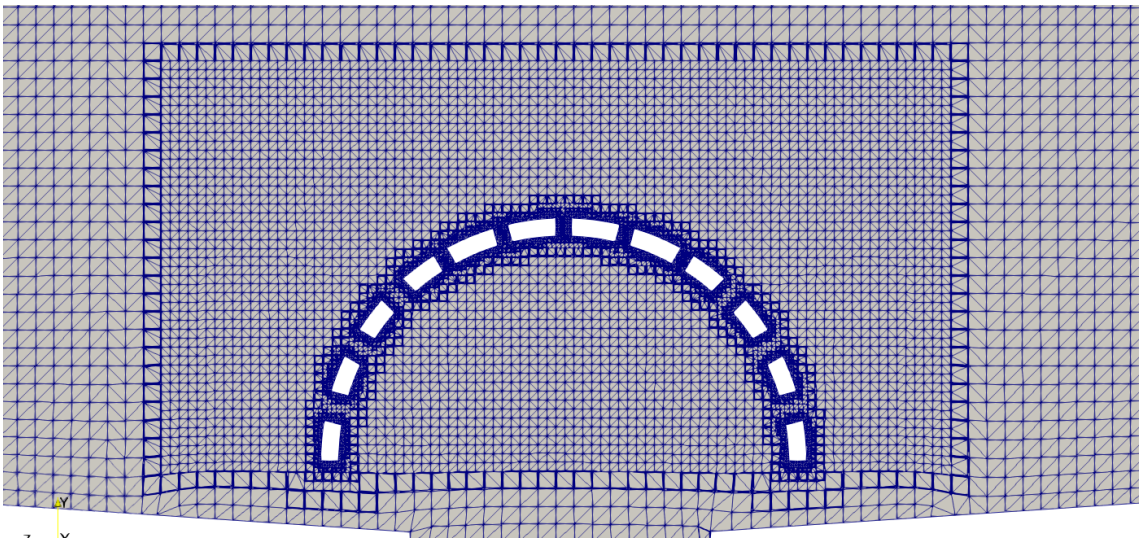

Figure 3.22. Mesh around deflector at LP2 tank.

This simulation, using an Intel® Core™ i7-5930K CPU @ 3.5GHz, at parallel processing using 12 cores, took about 25 days to process 15 seconds of flow. Results were saved every 0.2 seconds of simulated flow time.

At the first time recorded (0.2 seconds) everything seems to go well (see Annex T and Annex U). Free surface is symmetric to the geometrical symmetry plane of the tank, velocity profile at free surface too and the fluid is entering through the tube. At time 0.4 seconds, some unexpected results started appearing. Zones of high velocity show up inside and above the deflector. Also, velocity vectors shown at Annex U are not tangent to that plane, so, the flow is no longer symmetric. After this initial details, free surface begins

oscillating and even some jets of rubber are expelled from the free surface. Several times, rubber enter the inlet tube from the tank, taking the opposite trajectory to the expected that would happen. So, those computational results were no longer realistic. Such behaviour is odd, considering that the program only jumped to the next time step when the residuals achieved the tolerance defined (see Figure 3.23).

```
Time = 0.621659

PIMPLE: iteration 1
smoothSolver:  Solving for alpha.water, Initial residual = 7.38999e-10, Final residual = 7.38999e-10, No Iterations 0
Phase-1 volume fraction = 0.595483  Min(alpha.water) = 0  Max(alpha.water) = 1.00971
MULES: Correcting alpha.water
MULES: Correcting alpha.water
Phase-1 volume fraction = 0.595483  Min(alpha.water) = 0  Max(alpha.water) = 1.00971
DICPCG:  Solving for p_rgh, Initial residual = 0.000258154, Final residual = 1.11319e-05, No Iterations 7
time step continuity errors : sum local = 2.89557e-11, global = 2.15315e-14, cumulative = -1.19736e-05
DICPCG:  Solving for p_rgh, Initial residual = 0.000130022, Final residual = 5.46486e-06, No Iterations 9
time step continuity errors : sum local = 1.42296e-11, global = 2.51925e-14, cumulative = -1.19736e-05
DICPCG:  Solving for p_rgh, Initial residual = 4.34032e-05, Final residual = 9.91578e-08, No Iterations 194
time step continuity errors : sum local = 2.58734e-13, global = 6.62755e-14, cumulative = -1.19736e-05
smoothSolver:  Solving for omega, Initial residual = 1.46927e-05, Final residual = 8.99456e-09, No Iterations 1
smoothSolver:  Solving for k, Initial residual = 9.20309e-08, Final residual = 2.74513e-13, No Iterations 1
bounding k, min: -6.78174e-09 max: 0.318171 average: 0.0645704
ExecutionTime = 88135.6 s  ClockTime = 88530 s

fieldAverage Average write:
    Calculating averages

Courant Number mean: 5.91871e-07 max: 0.879447
Interface Courant Number mean: 1.6877e-08 max: 4.48663e-05
deltaT = 1.41572e-07
```

Figure 3.23. Output text for a timestep.

To solve this problem, it could be added under-relaxation or decreased tolerances. Also, a 3D simulation with a vertical inlet could have been performed to see its influence. As such simulation would take around 25 days, a step back to 2D simulations was decided.

3.2.3.2. LP2 2D with deflector

A new 2D simulation (LP2_2D) was done assuming the geometry of a cut in the middle of the tank, as made for Figure 3.21, including the deflector cut also. So, an infinite length in the X direction is assumed, transforming the semi-spherical geometry into a semi cylinder.

The mesh around the deflector, constructed in a similar way to the 3D simulation, is shown in Figure 3.24.

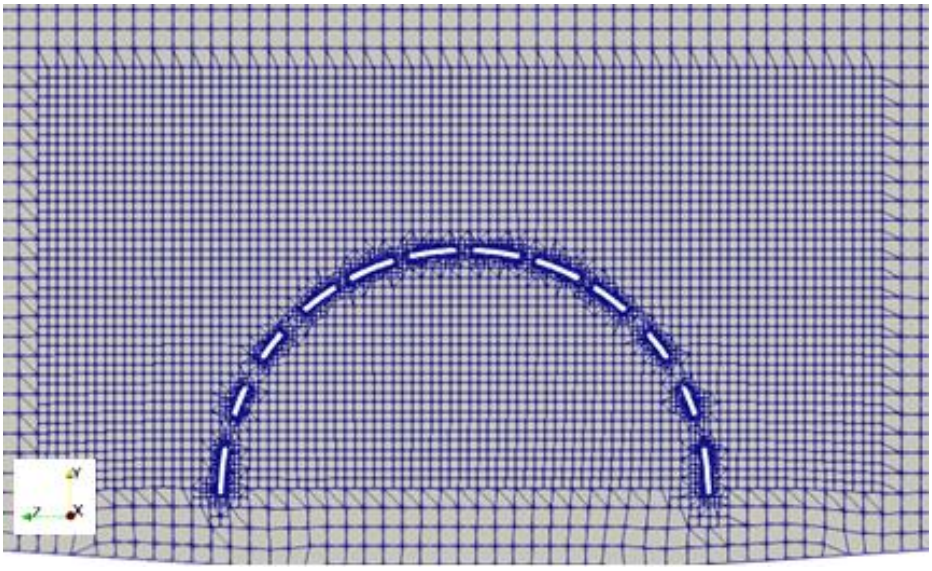

Figure 3.24. Mesh around deflector for LP2_2D.

The results of the present 2D case show a much more stable behaviour relatively to the 3D simulation mentioned in Section 3.2.3.1. After 10 seconds of simulation, the solution converged to a steady state.

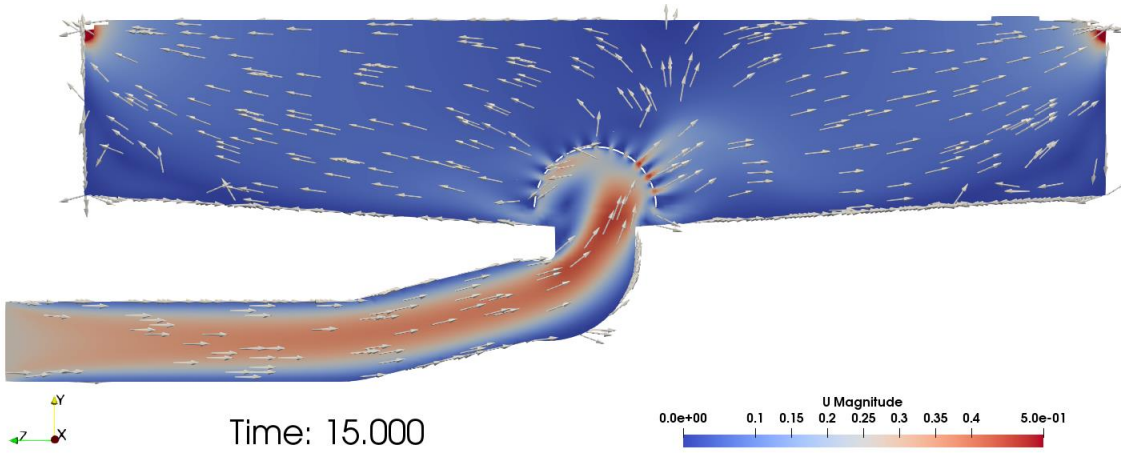

Figure 3.25. Velocity field for LP2_2D.

Inside the entrance tube, the velocity profile takes the same tendency as if no deflector was present. However, near the deflector, the inlet jet is, due to a higher-pressure zone (see Figure 3.26), dispersed into radial directions, inducing a larger zone of high velocity, as shown in Figure 3.25. Velocity and pressure, outside the deflector, don't change much. The lowest velocities appear at 3 zones. A stagnation point appears near the free surface but, with the flow entering from the centre of the tank, that can't be cancelled. The other 2 zones, of lowest velocities, are located by the lower corners of the tank. Those zones

represent recirculation bubbles, that could be eliminated with a curved plate placed above those regions. A small swallow appears at the free surface, for negative Z's.

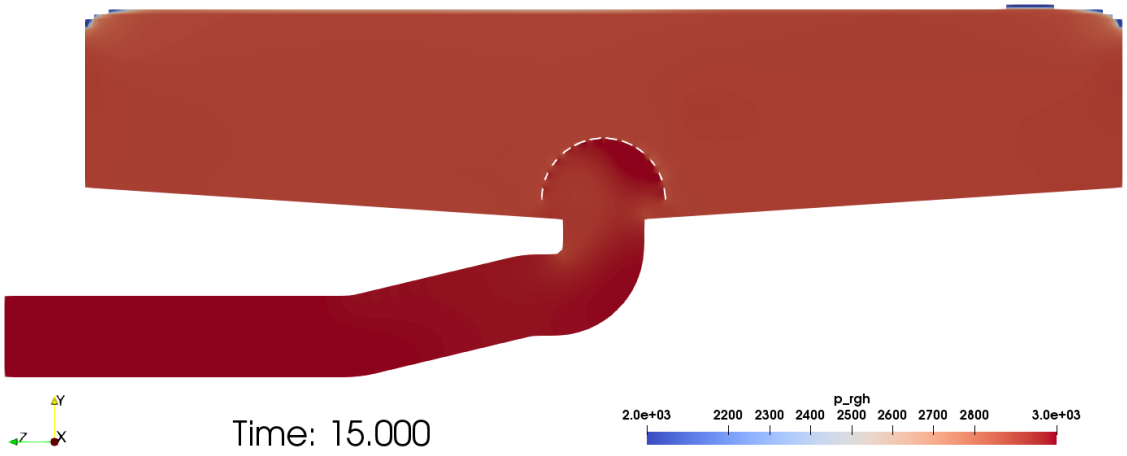

Figure 3.26. Pressure field for LP2_2D.

As the flow that comes from the tube has a horizontal component of velocity, it impinges on the deflector with higher velocity on the right hand, as illustrated in Figure 3.27, creating the zone of higher pressure. The secondary jets, for that reason, are stronger there, and more fluid is directed to that side of the tank. This is the reason why the small swallow appears. The smaller holes at the top part of the deflector seem big enough to feed the zone above the deflector without creating any swallow.

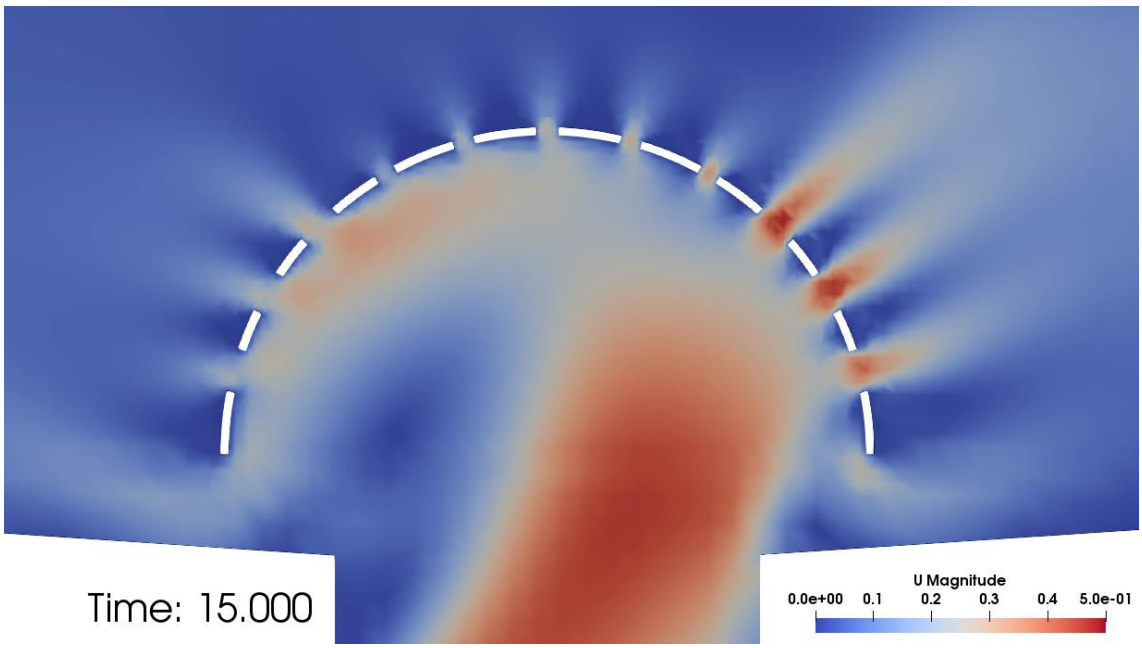

Figure 3.27. Velocity magnitude near deflector for LP2_2D.

3.2.3.3. LP2 2D with deflector and vertical inlet

Another simulation, called here LP2_2D_V, was set, like the one in the previous section, but with a vertical inlet tube. Considering an inlet Reynolds number of 130 and a diameter of 0.1 m, using equation (2.1), the tube length, to achieve a fully established flow inside it, is 0.99 m, here rounded to 1 m. Again, the main mesh is composed by 6 mm cubes, with the refinements exemplified at Figure 3.24.

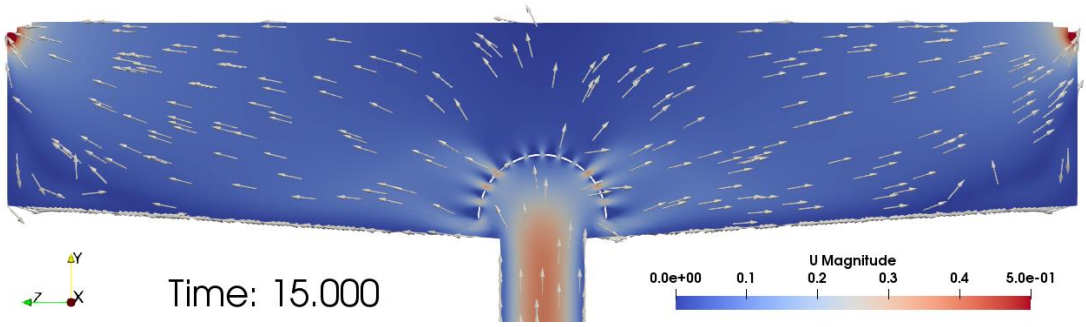

Figure 3.28. Velocity field for LP2_2D_V.

With the vertical inlet tube, some differences, relatively to the case presented in Section 3.2.3.2, were noticed. As the deflector blocks partially the flow that enters the tank, a higher-pressure zone is set inside of it, as observed in Figure 3.29, and the flow reduces its velocity when entering that region. Outside the deflector, the flow seems symmetric. As Figure 3.28 shows, a large zone of reduced velocity appears on each side. So, the fluid is not only projected through the bottom of the tank but is spread throughout all domain. Again, above the deflector, velocity is lower, for the same reasons presented in previous section. Near the lower corners, as in the simulation of Section 3.2.3.2, recirculation zones exist. In this case there is no swallow on the free surface.

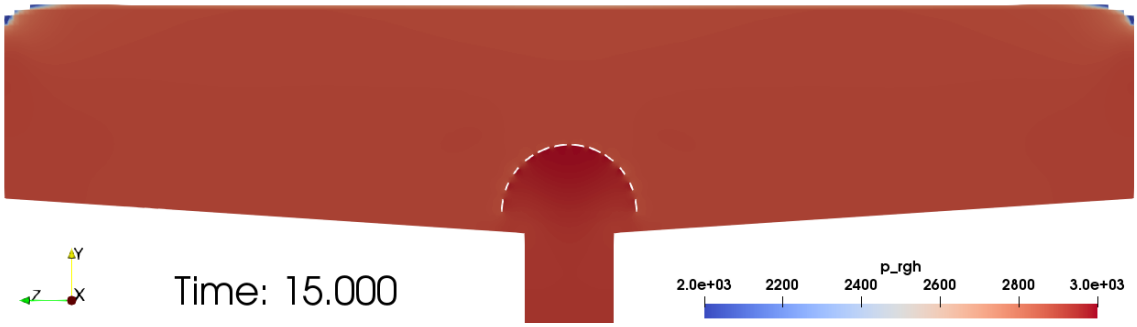

Figure 3.29. Pressure field for LP2_2D_V.

Near the deflector flow is also symmetric. Again, as the bottom holes are larger, velocity of the secondary jets created there is higher (see Figure 3.30). This creates irrigation

enough to spread fluid to the sides. Holes at the top, again, feed the zone above the deflector, preventing the formation of a swallow above the main jet.

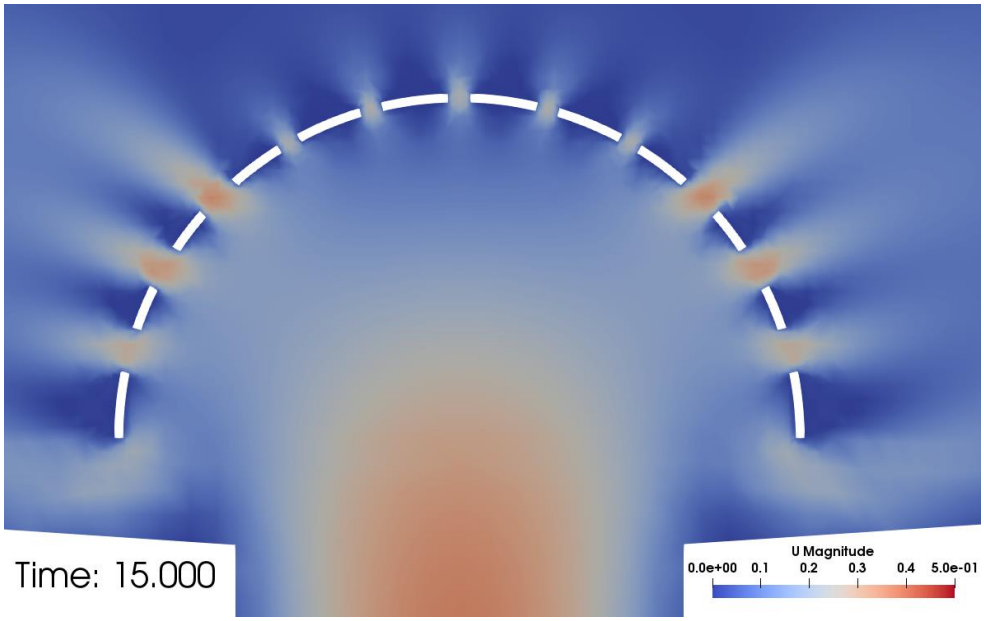

Figure 3.30. Velocity field near deflector for LP2_2D_V.

4. CONCLUSIONS

The present work aimed at the development of a solution of a manufacturing problem occurring in Ansell, Vila Nova de Poiares. In specific, it intends to develop a dispositive to prevent the formation of non-horizontal free surface in tanks where gloves are dipped in a solution, a process from which rejected products are susceptible to occur.

From this work, subdivided in two main sections, the following conclusions were withdrawn:

4.1. Validation

Validation became a substantial part of this work. In it, the results from OpenFOAM® were benchmarked against the experimental values in Espa and Frattini (2002). From all the turbulence models used, the most realistic results, in terms of free surface oscillation, were obtained using the k-ω SST model. For the first study made, it was also the one which approximated better the frequency of oscillation.

During the mesh refinement, the frequency of oscillation did not behave as expected. As mesh was refined, the frequency of oscillation discrepancy relatively to the experimental increased. Improvements were obtained by modifying the convergence criteria. The decreasing of convergence tolerances was efficient, as the frequency of oscillation got a final error to the real of 1.412%. 3D simulations were not possible with the selected 2D mesh due to computational restrictions.

With the optimal simulation parameters, the free surface shape and oscillation of the jet were in good agreement with the real flow. However, better results were expected in zones away from the jet.

4.2. Development of the factory tank

The optimal parameters were selected to study the effect of several deflector geometries. With plane plates, the oscillation of the main jet was removed. It was found that the zone above the deflector must be fed with fluid to prevent the formation of recirculation

zones near the free surface. So, holes, preferentially orientated in different directions, are recommended. Besides that, plane plates always induced high velocity zones near the bottom of the tank, preventing the deposition of rubber. These conclusions were useful for the design of geometry of the final deflector.

The increase of the distance of the deflector to the bottom of the tank obviated the recirculation zones near the free surface, which is a clear improvement. But that distance is limited by the height of the deflector and the deepness of the gloves when immersed.

The results from the 3D simulation are slightly different from those of the 2D case. The swell is still predicted, but now without oscillation. The recirculation zones near the jet remain, although smaller. However, those results aren't really conclusive because of the lack of experimental data for the benchmark.

The 3D simulation performed for the LP2 tank configuration, without the deflector, despite of a good prediction of the swell location, showed large discrepancies relatively to other onsite observations. So, a review of the 3D results is necessary.

The implementation of the optimized deflector in a 2D situation revealed that its geometry offers a uniform feeding of all the zones of the tank, with no problematic recirculation regions, namely those near the bottom eliminated by rounding the edges.

It was observed that the real inlet tube origins a non-vertical main jet. This means that one side of the tank gets a larger amount of fluid, resulting in a swallow on that side. This could be solved. A longer vertical inlet tube is not possible, as there are space limitations, so, corner vanes at the elbow could be used. However, some caution to the distance between the plates is necessary, as clogging problems can appear.

About the semi-spherical geometry nothing can be concluded as the 3D simulation did not provide realistic results. Nevertheless, from the 2D simulations made, it was inferred that the semi-spherical deflector might be a useful solution. Some additional dimensional adjustments may be necessary, and further 3D simulations are necessary, which is suggested for future work.

For the adoption of a LES model, to compare those results with RAS results, finer meshes would be necessary, which would require a longer processing time unviable to 3D simulations. The use of such models, in 2D simulations, is also suggested for future work.

BIBLIOGRAPHY

Auld, D.J. and Srinivas, K. (1995), "Aerodynamics for students", Accessed at 2018 February 15th at: http://www-mdp.eng.cam.ac.uk/web/library/enginfo/aerothermal_dvd_only/aero/contents.html

Espa, P. and Frattini, A. (2002), "Experimental study of turbulent, 2-D, vertical jets in shallow water", Proceedings of the 11th International Symposium on Applications of Laser Techniques to Fluid Mechanics, 36.6, Lisbon, 2002.

Fukaya, M., Madarame, H. and Okamoto, K. (1996), "Growth mechanism of self-induced sloshing caused by vertical plane jet", Proceedings of International Conference of Nuclear Engineering (ICONE-4), Vol. 1, 781-787.

Greenshields, C.J. (2017, July 24th), "OpenFOAM User Guide", version 5.0.

Kuang, J., Hsu, C. and Qiu, H. (2001), "Experiments on vertical turbulent plane jets in water of finite depth", Journal of Engineering Mechanics, 127, 18-26.

Madarame, H. and Iida, M., (1998), "Mechanism of jet-flutter: self-induced oscillation of an upward plane jet impinging on a free surface", JSME International Journal, Series B, Vol. 41, No.3, 610-617.

Madarame, H., Okamoto, K. and Iida, M. (2002), "Self-induced sloshing caused by an upward round jet impinging on the free surface", Journal of Fluids and Structures, 16(3), 417-433.

Mata-Lima, H., Cristina, R., Silva, V.V. (2008), "Controlo do Escoamento e Medição de Caudais: Critérios de dimensionamento de descarregadores em canais, colectores e pequenas represas", Engenharia Civil journal, 30, 51-66.

Wu, S., Rajaratnam, N. and Katopodis, C. (1998), "Oscillating vertical plane turbulent jet in shallow water", Journal of Hydraulic Research, 36, 229-234.

ANNEX

```
convertToMeters 1;

vertices
(
    (-0.500  -0.525  -0.0105) //0
    ( 0.500  -0.525  -0.0105) //1
    ( 0.500   0.268  -0.0105) //2
    (-0.500   0.268  -0.0105) //3
    (-0.500  -0.525   0.0105) //4
    ( 0.500  -0.525   0.0105) //5
    ( 0.500   0.268   0.0105) //6
    (-0.500   0.268   0.0105) //7
);

blocks
(
    hex (0 1 2 3 4 5 6 7) (280 236 1) simpleGrading (1 1 1)
);

edges
(
);

boundary
(
    atmosphere
    {
        type patch;
        faces
        (
            (2 3 7 6)
            (0 1 5 4)
            (1 2 6 5)
            (0 4 7 3)
        );
    }

    frontback
    {
        type empty;
        faces
        (
            (0 3 2 1)
            (4 5 6 7)
        );
    }
);

mergePatchPairs
(
);
```

Annex A. *blockMesh* dictionary's code.

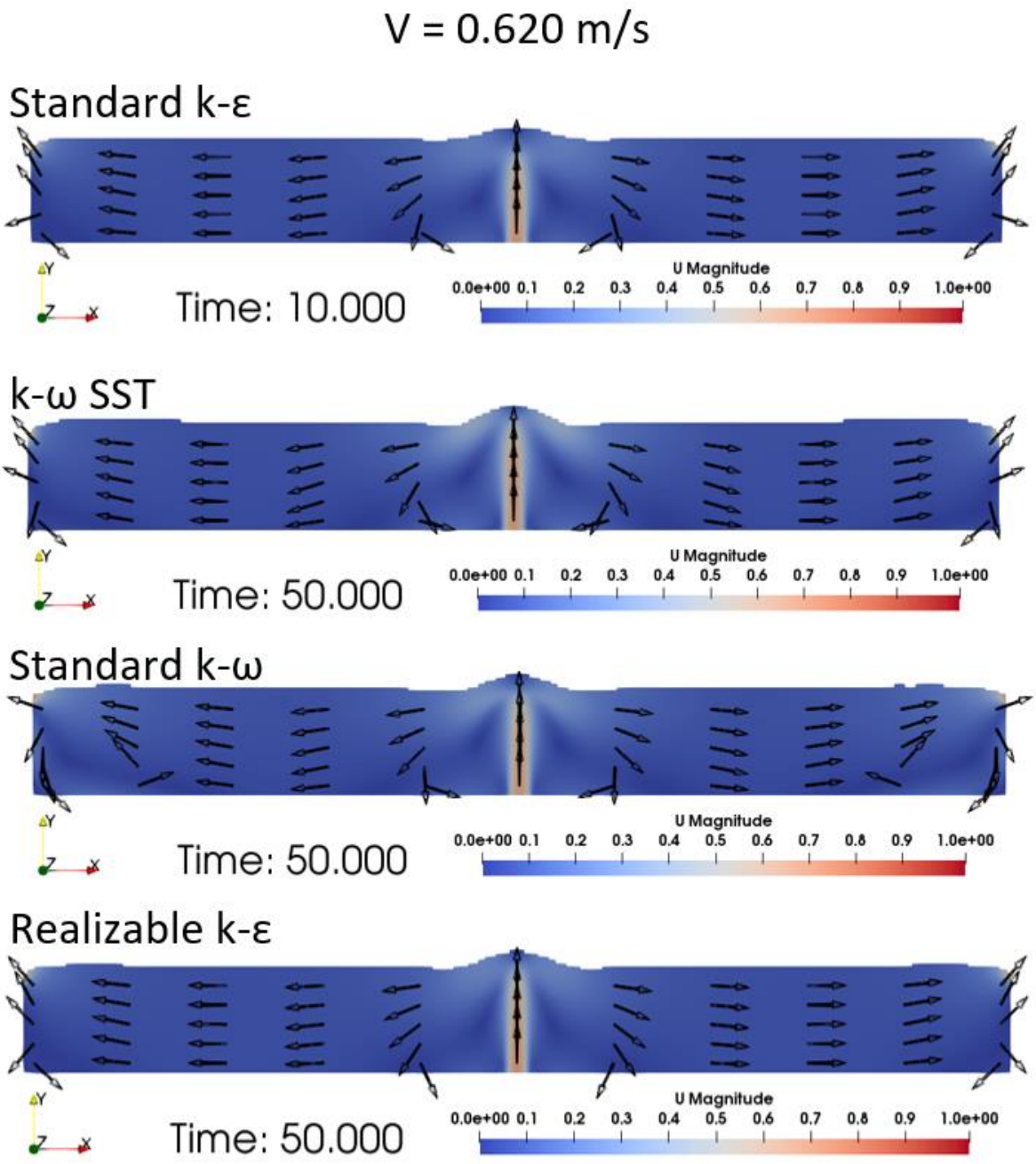

Annex B. Velocity profile for several turbulence models at latest timestep (t=50 seconds), V=0.620 m/s.

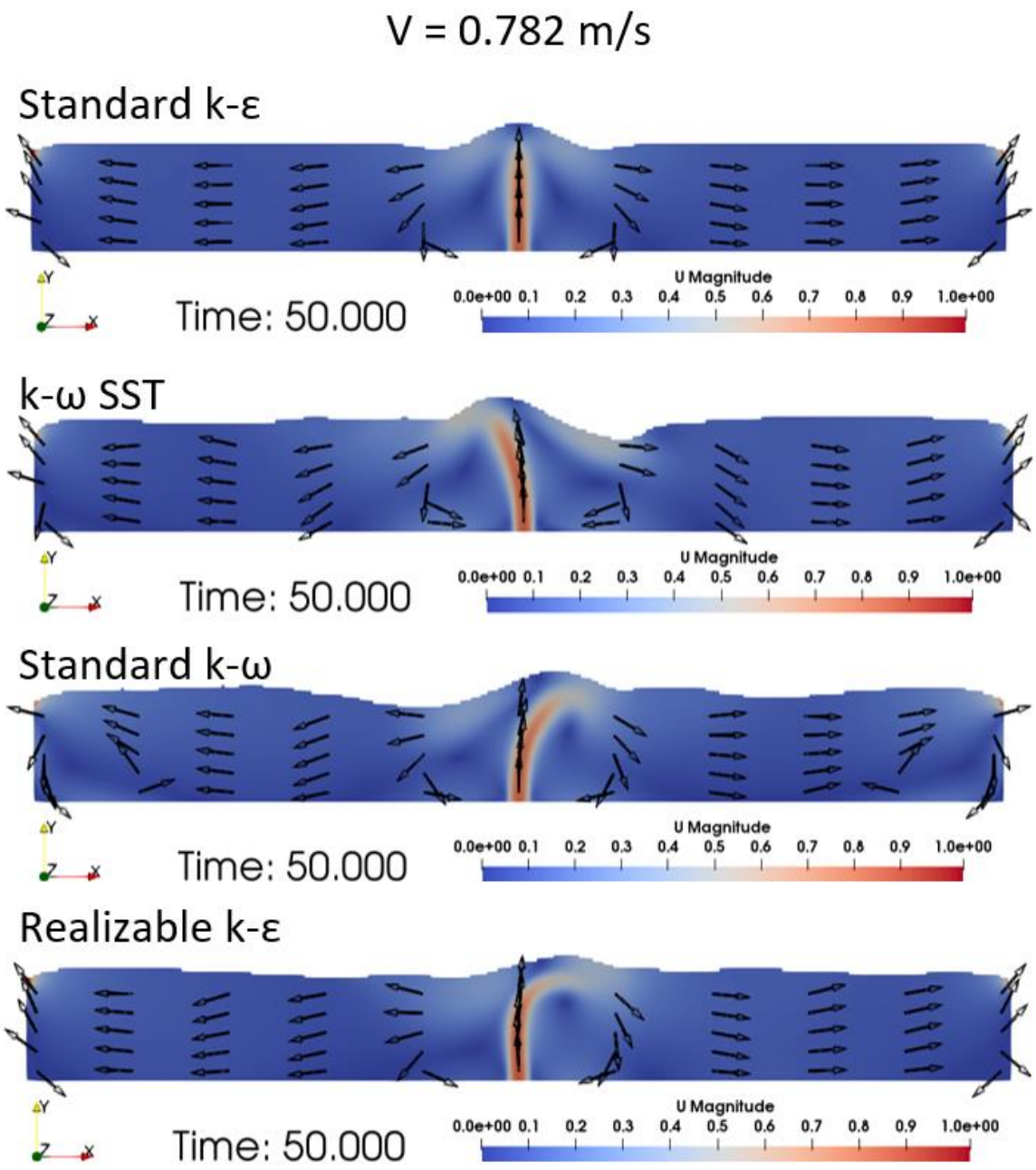

Annex C. Velocity profile for several turbulence models at latest timestep (t=50 seconds), V=0.782 m/s.

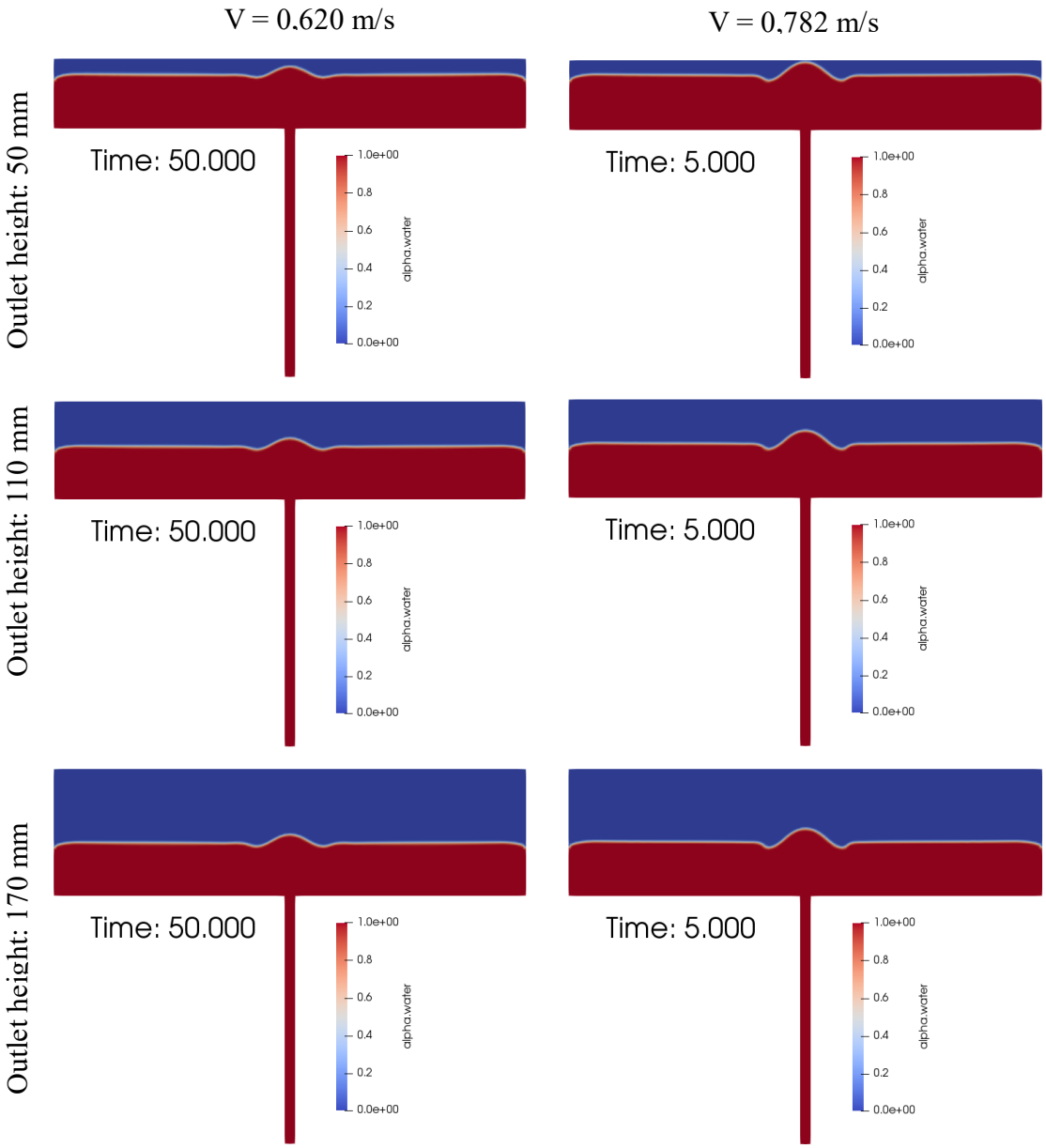

Annex D. Stability of free surface at timesteps when samples were taken.

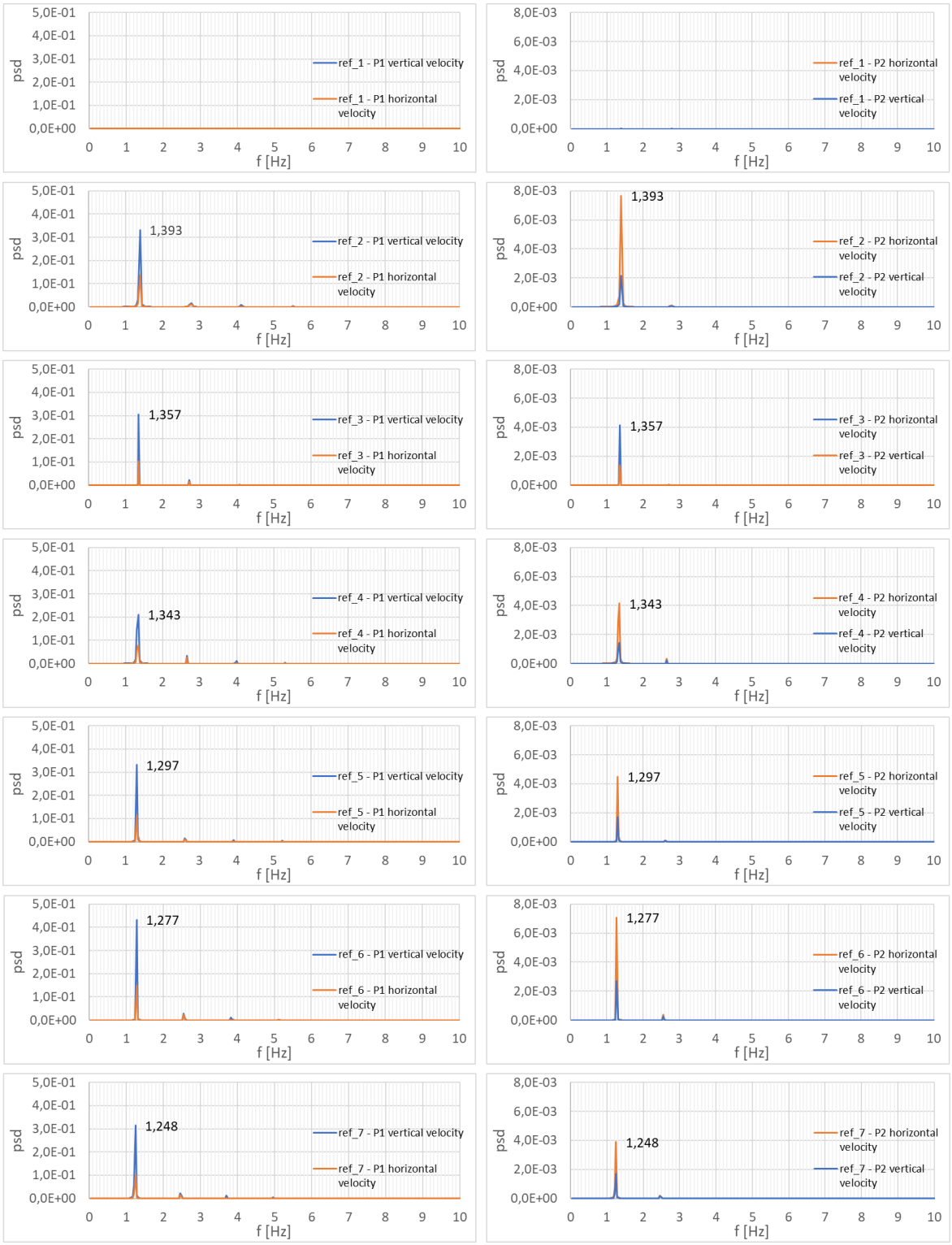

Annex E. *psd* results from mesh refinement study.

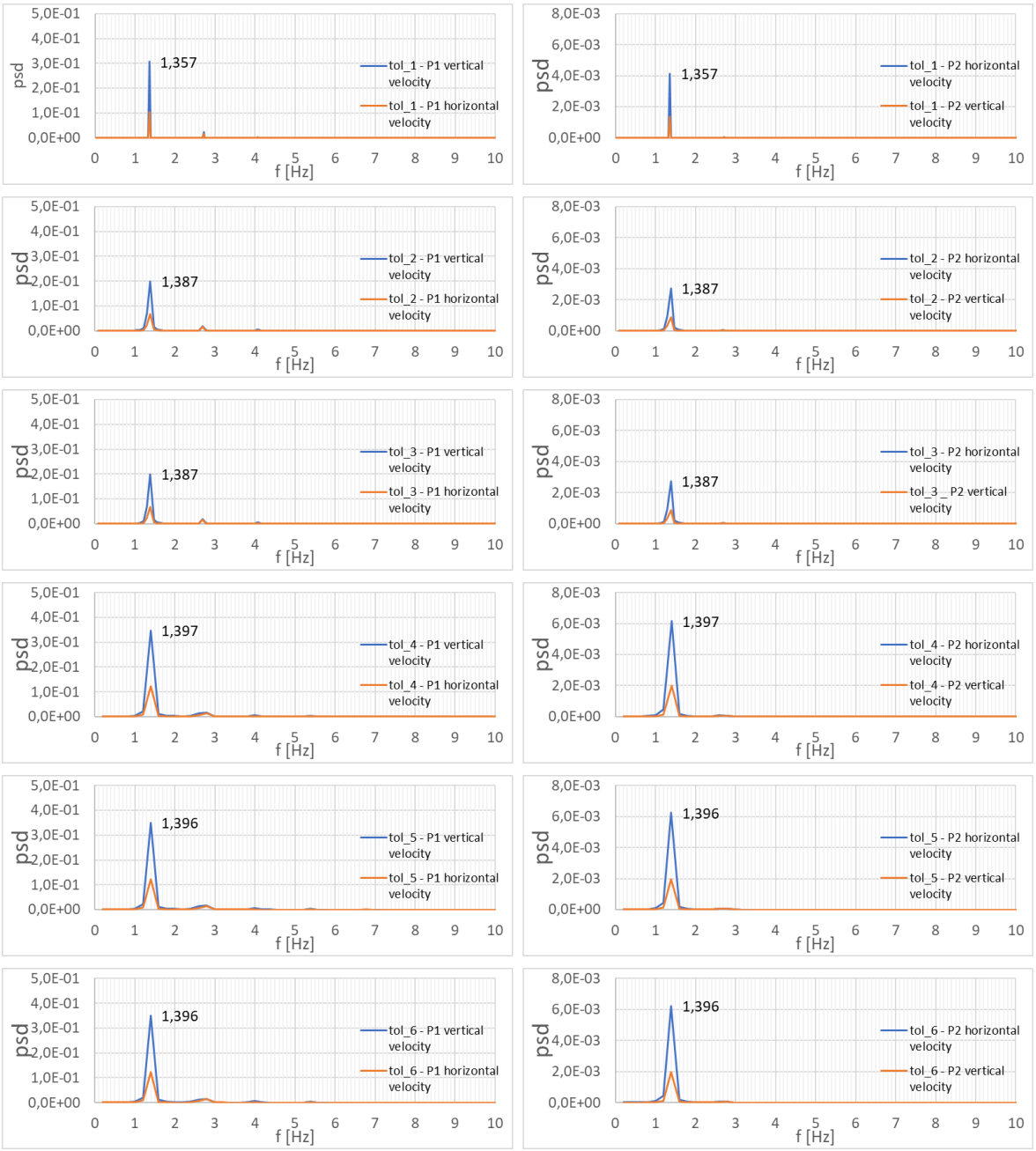

Annex F. *psd* results from tolerance modifications.

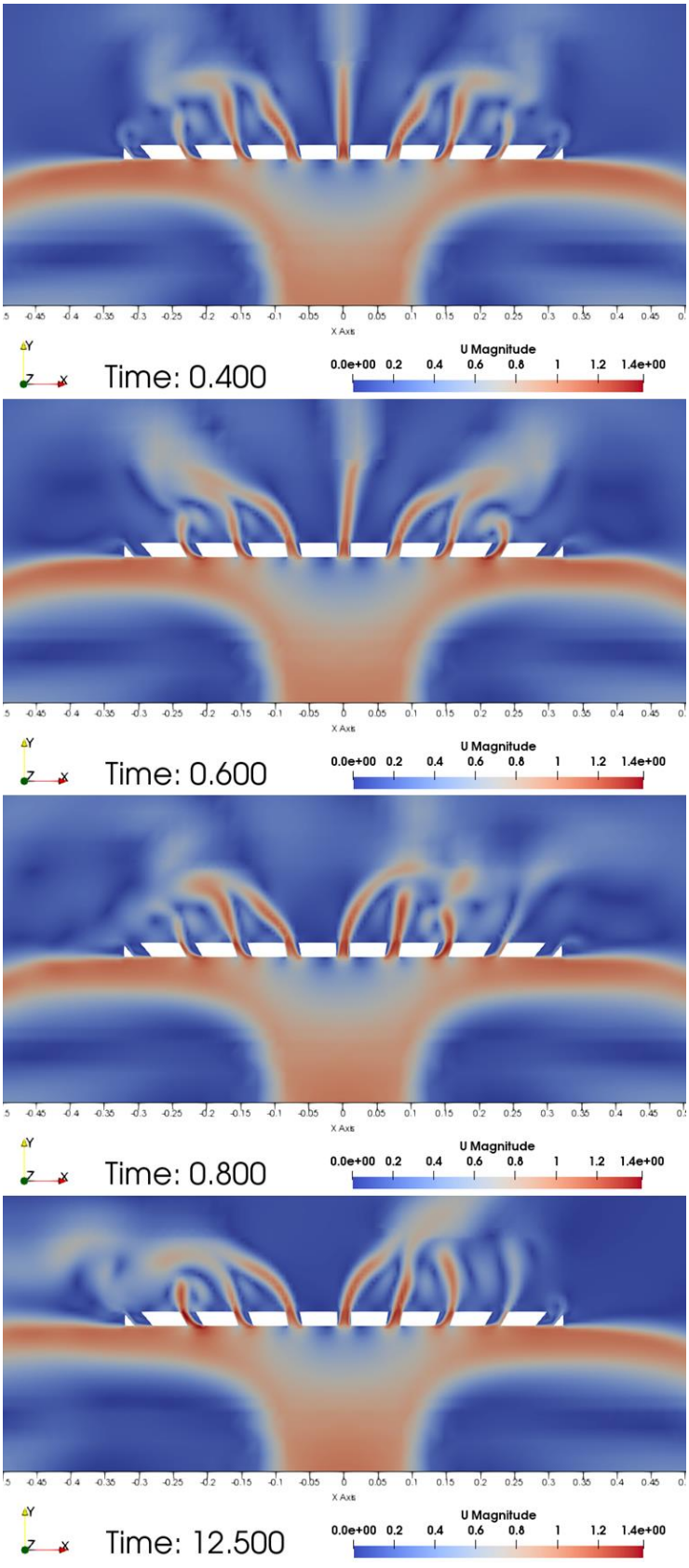

Annex G. Inclination of central jet to one of the sides.

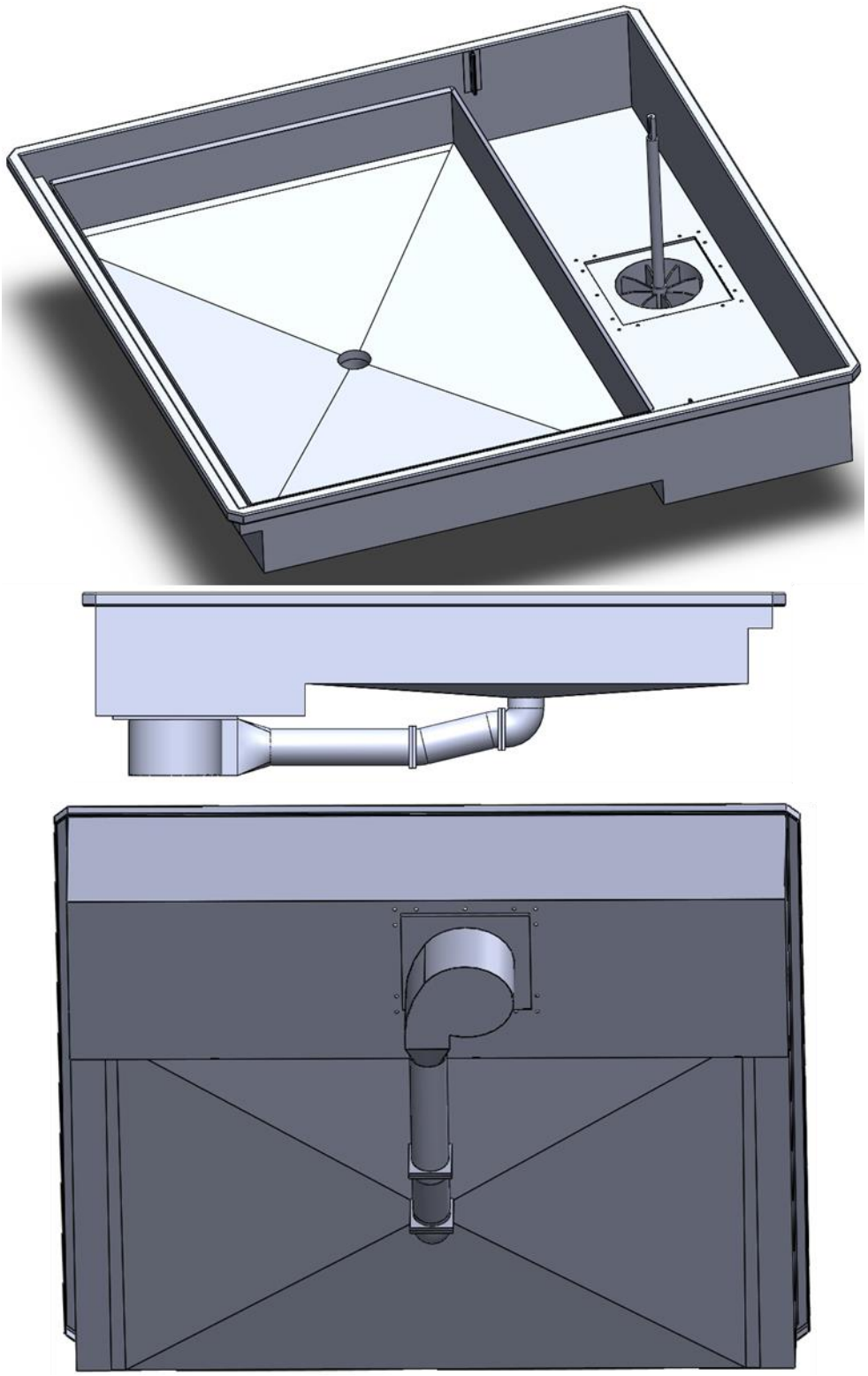

Annex H. LP2 tank geometry.

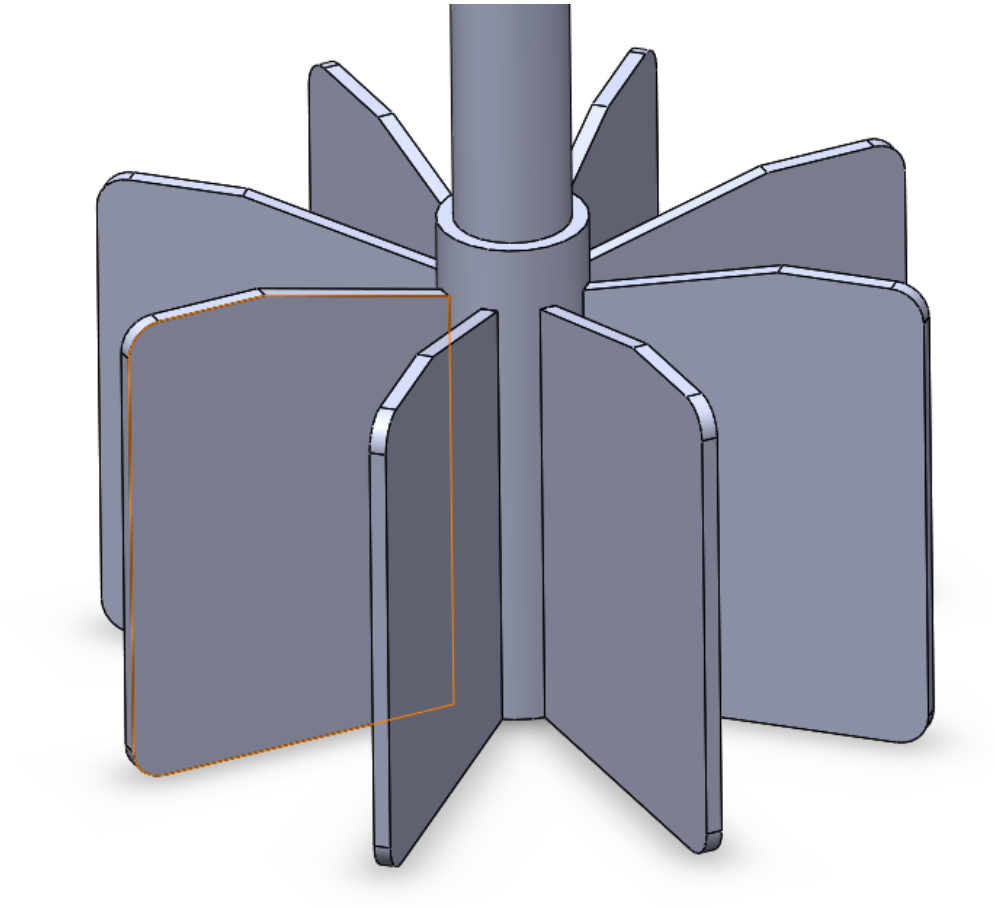

Annex I. Pump's rotor geometry.

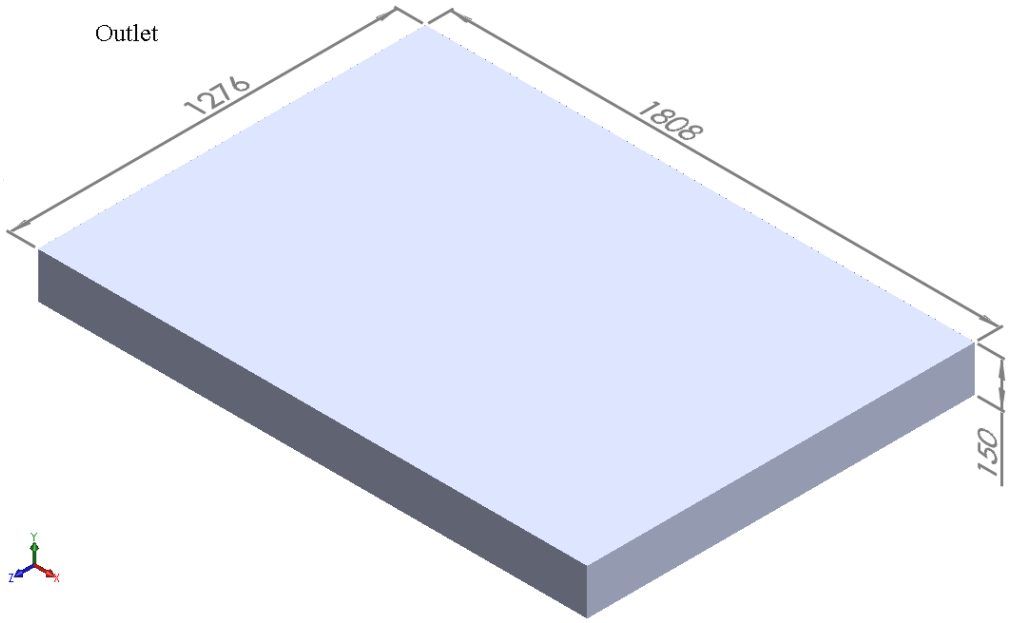

Annex J. Outlet geometry and dimensions (in mm) for LP2 3D simulations.

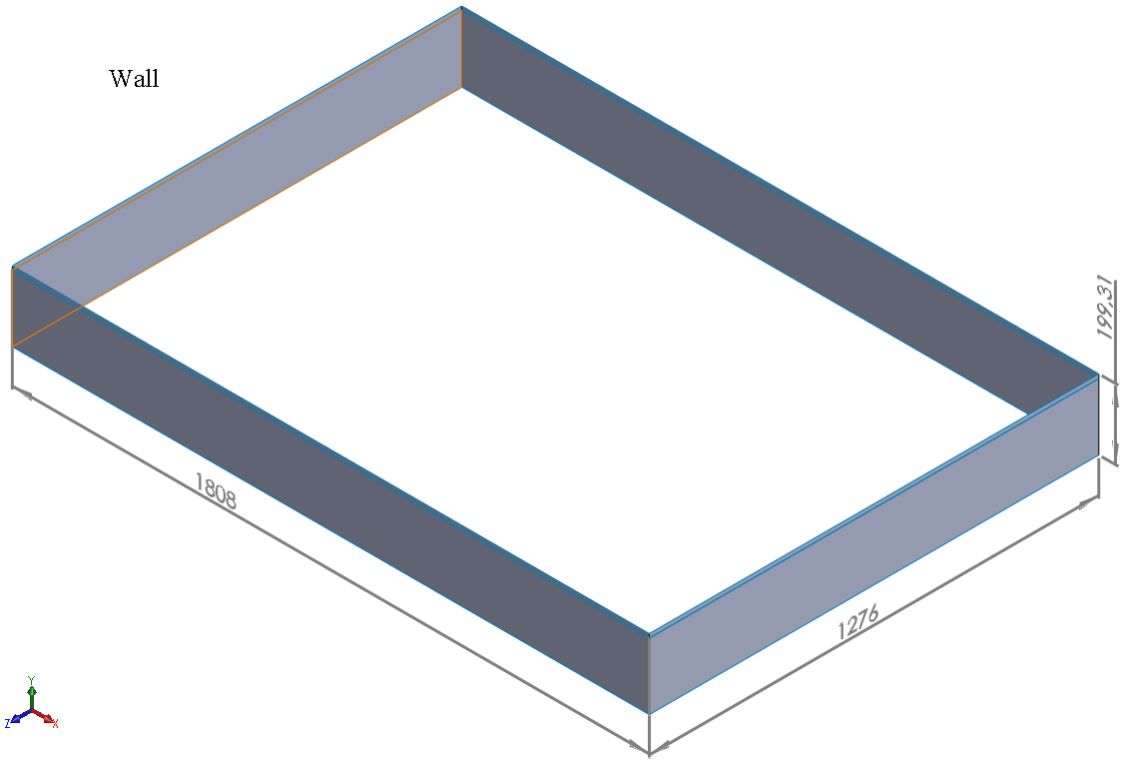

Annex K. Wall geometry and dimensions (in mm) for LP2 3D simulations.

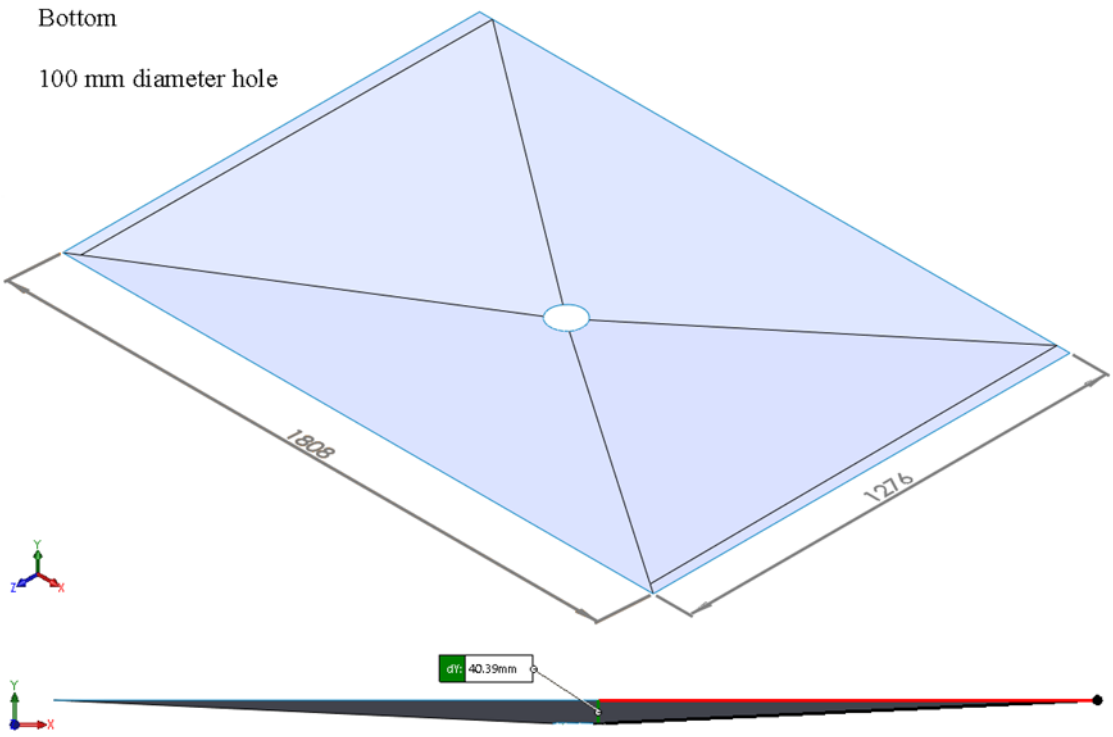

Annex L. Bottom geometry and dimensions (in mm) for LP2 3D simulations.

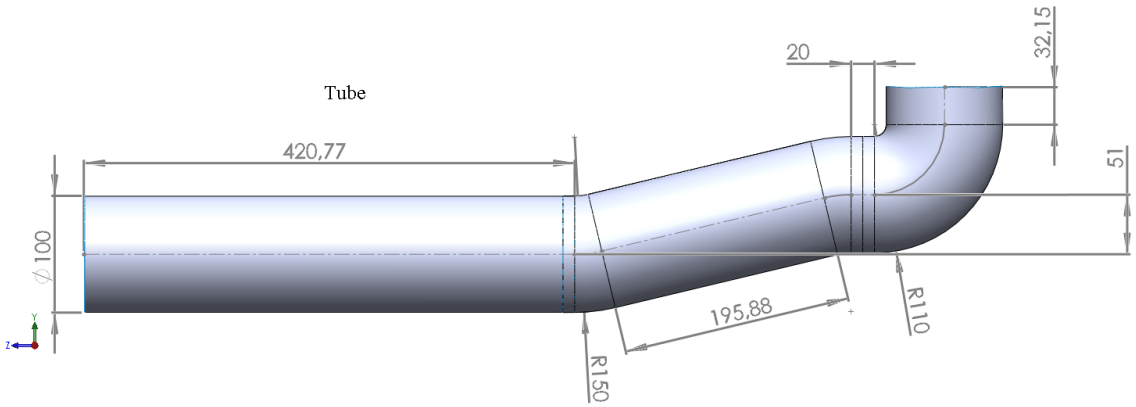

Annex M. Bottom geometry and dimensions (in mm) for LP2 3D simulations.

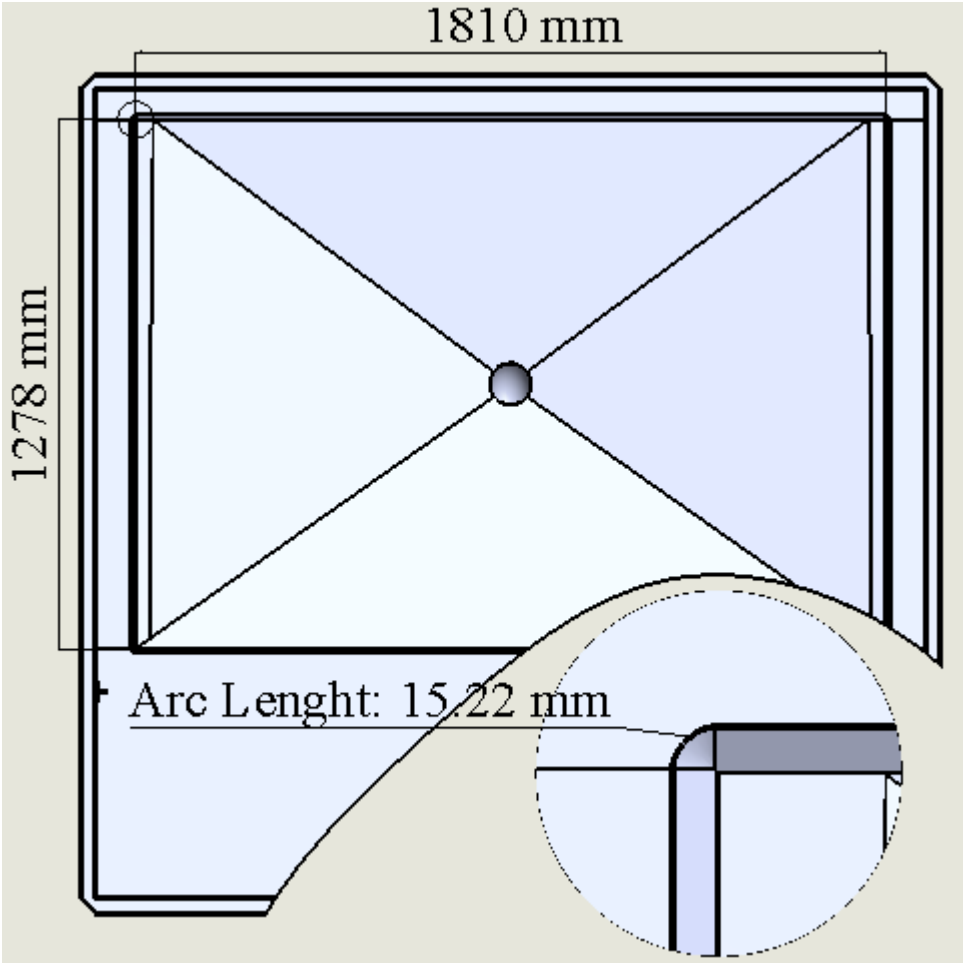

Annex N. Dimensions relative to the perimeter of the weir (LP2 tank).

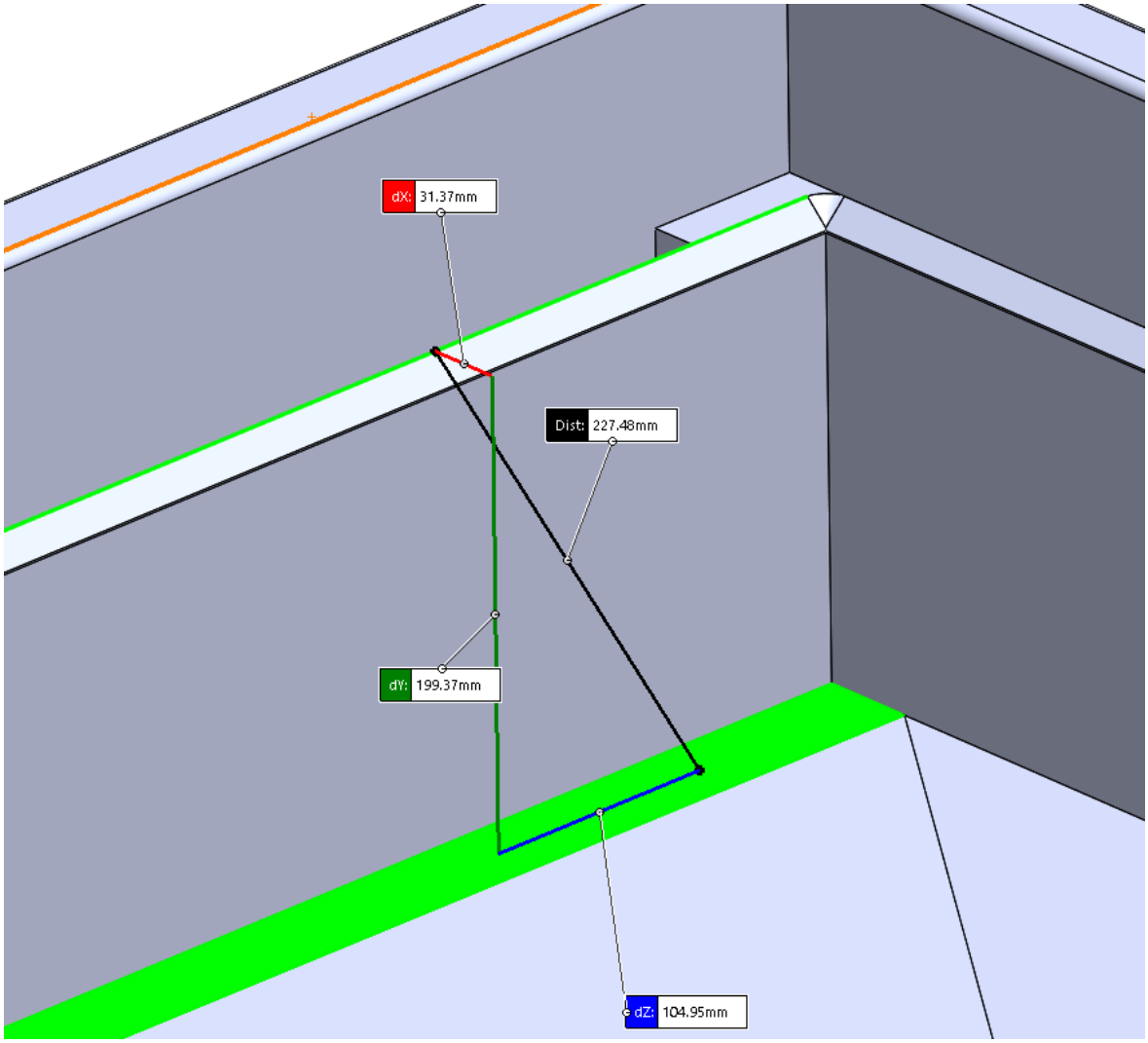

Annex O. Height of the weir relatively to the bottom of the LP2 tank.

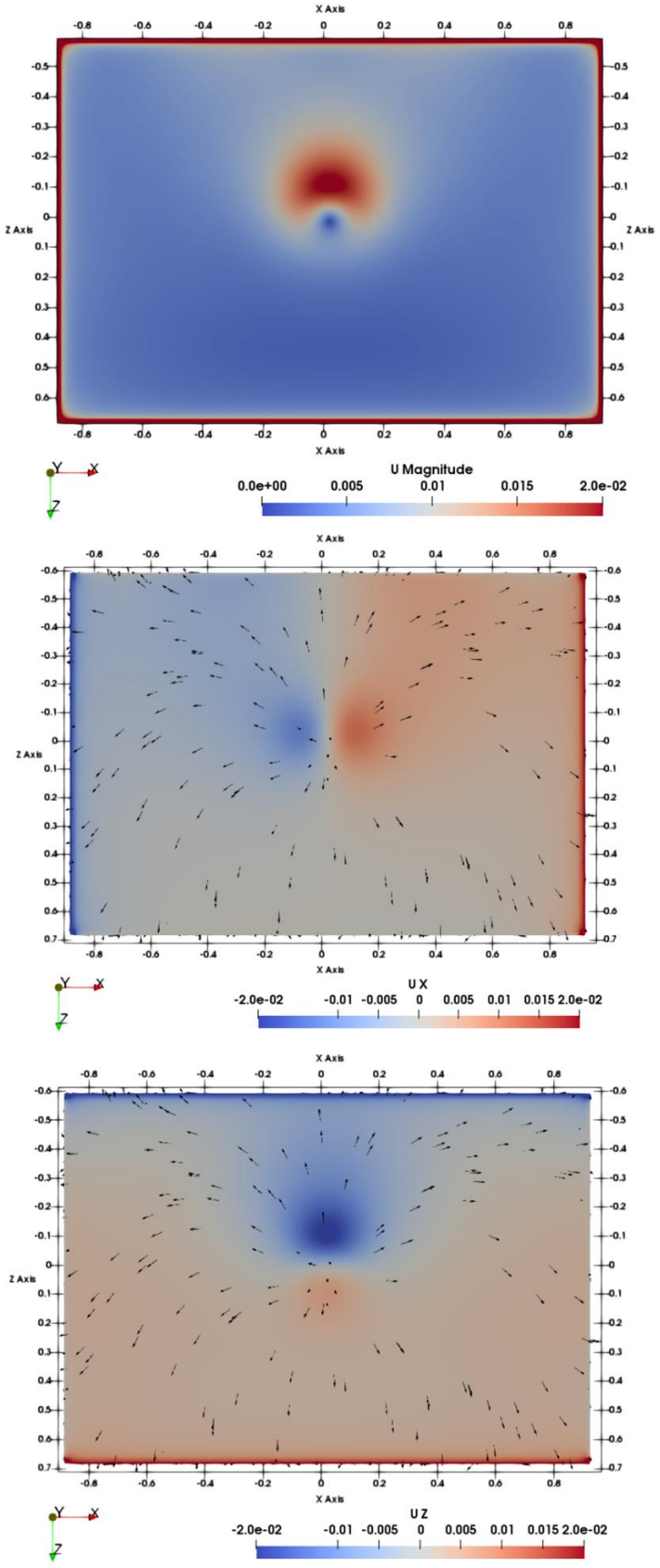

Annex P. Velocity fields at free surface of LP2 tank's simulation at 15 seconds (dimensions in m).

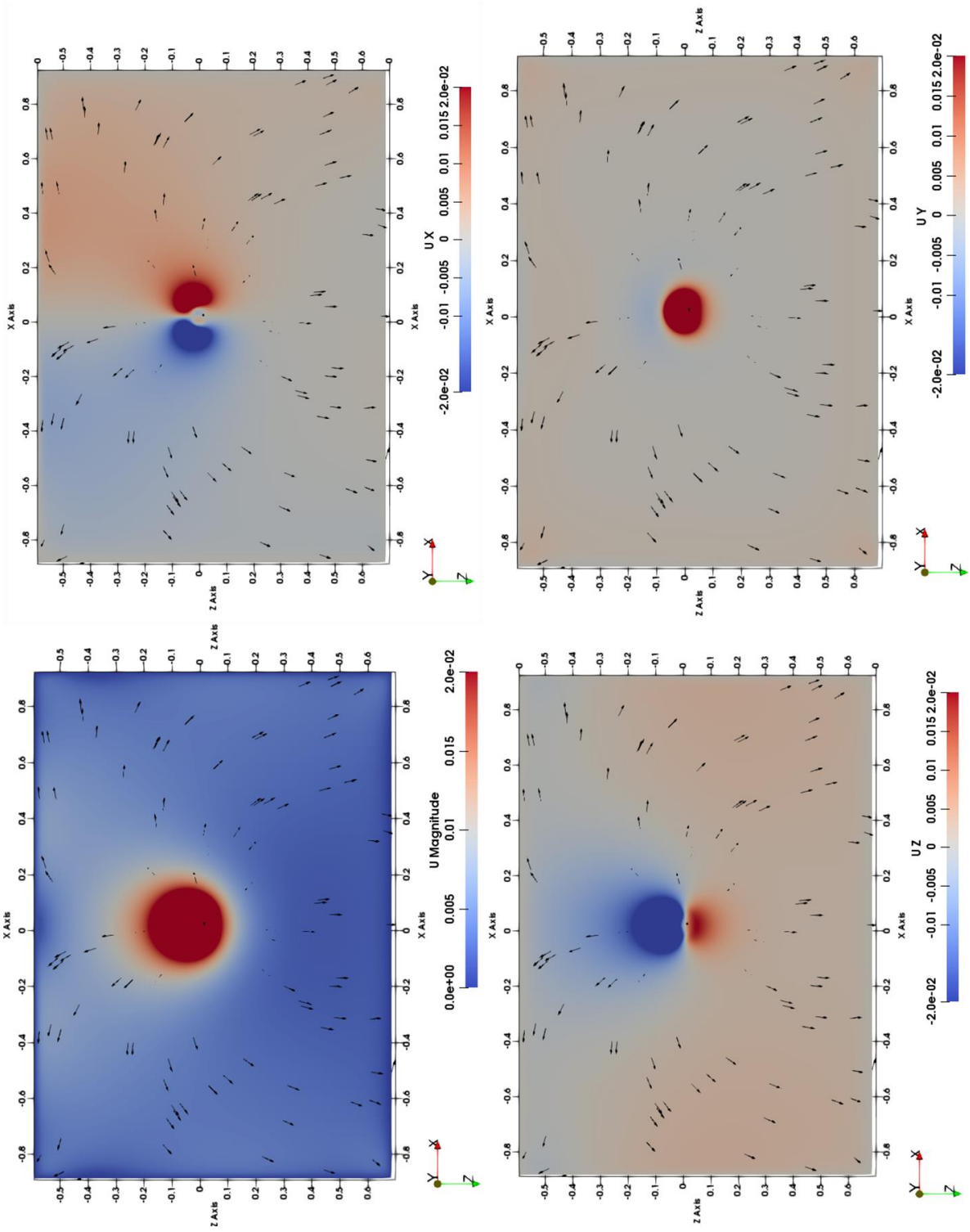

Annex Q. Velocity fields at Y=0.17 m of LP2 tank's simulation at 15 seconds (dimensions in m).

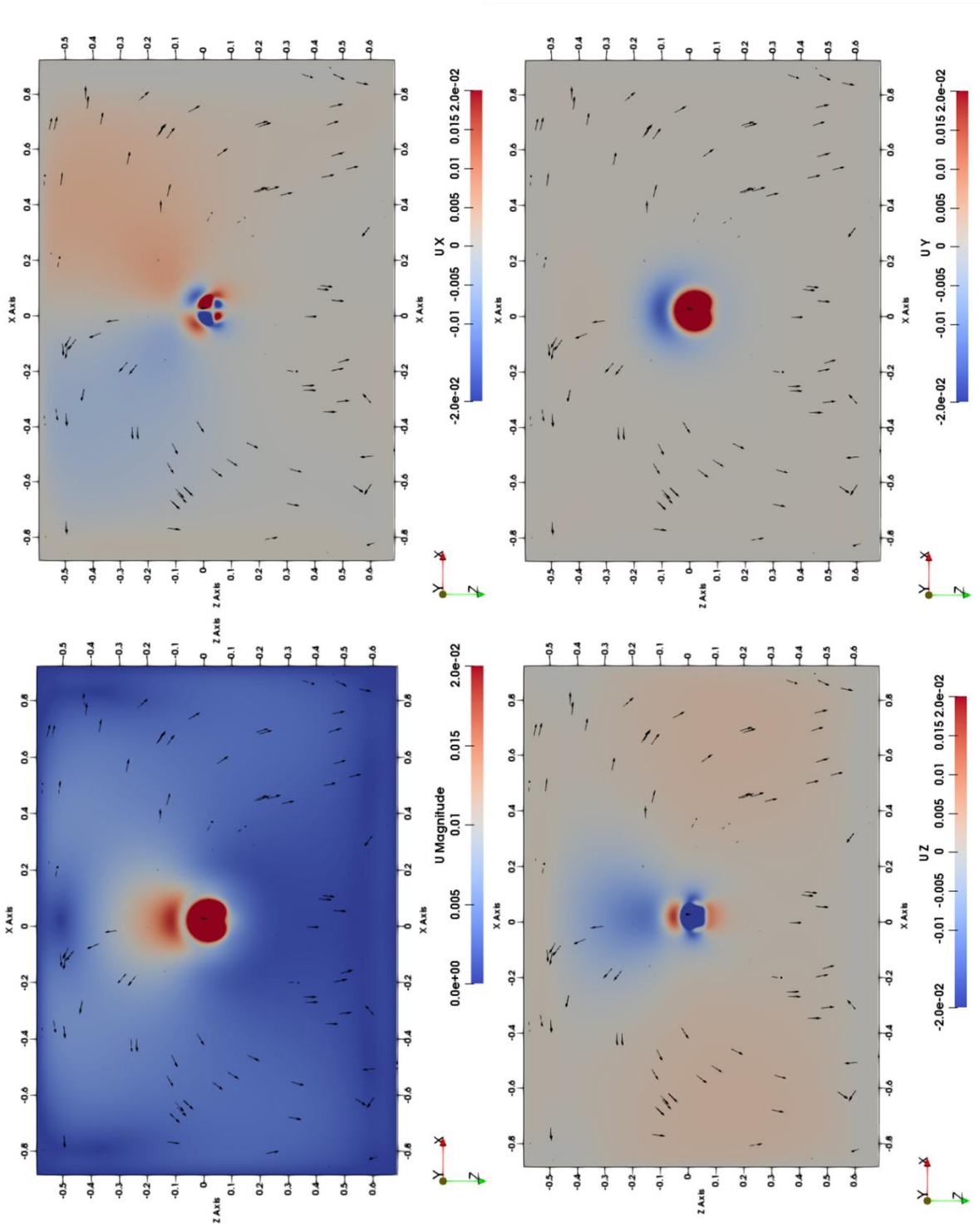

Annex R. Velocity fields at Y=0.09 m of LP2 tank's simulation at 15 seconds (dimensions in m).

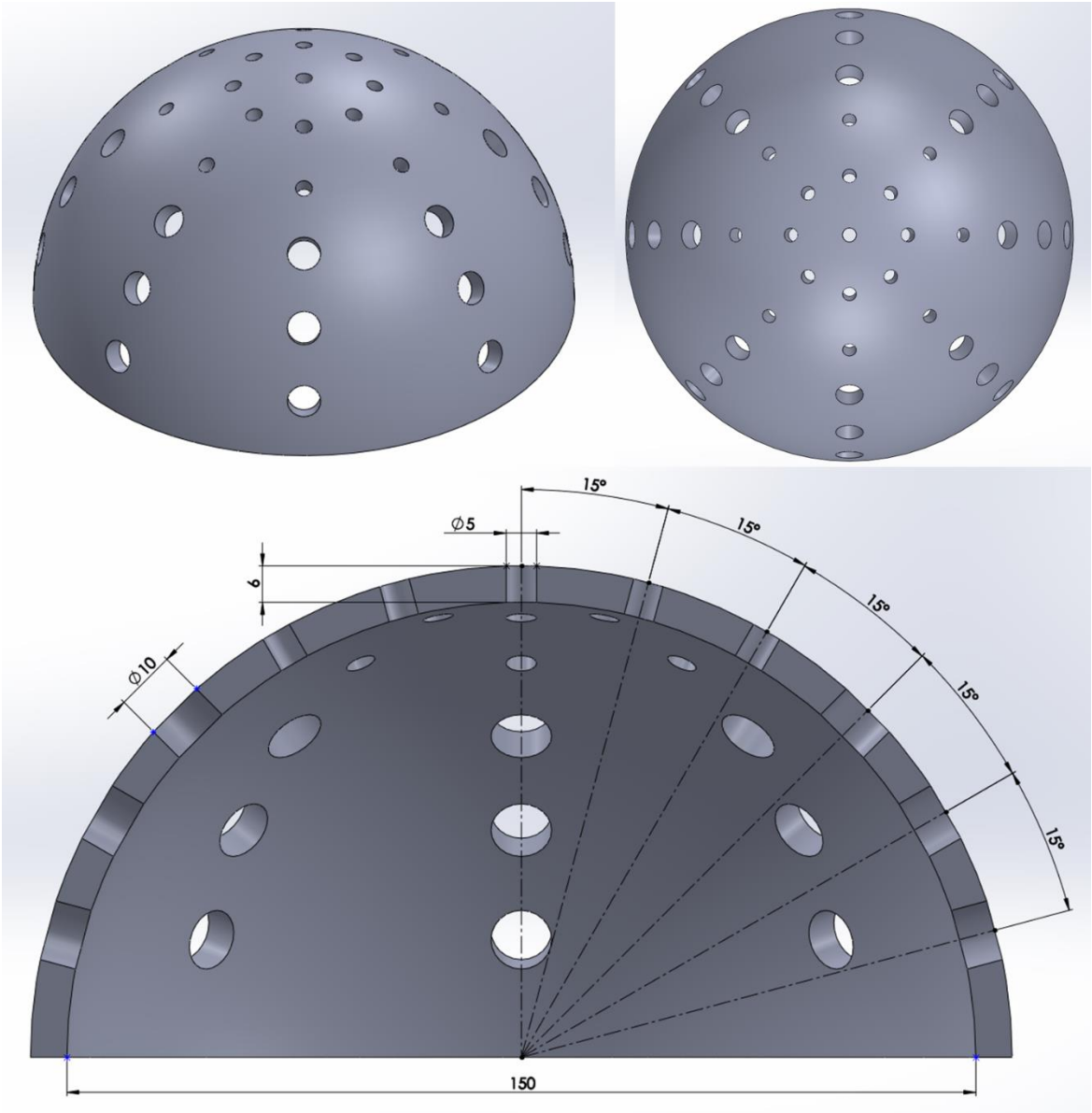

Annex S. Geometry of deflector used in LP2 tank simulation (dimensions in mm).

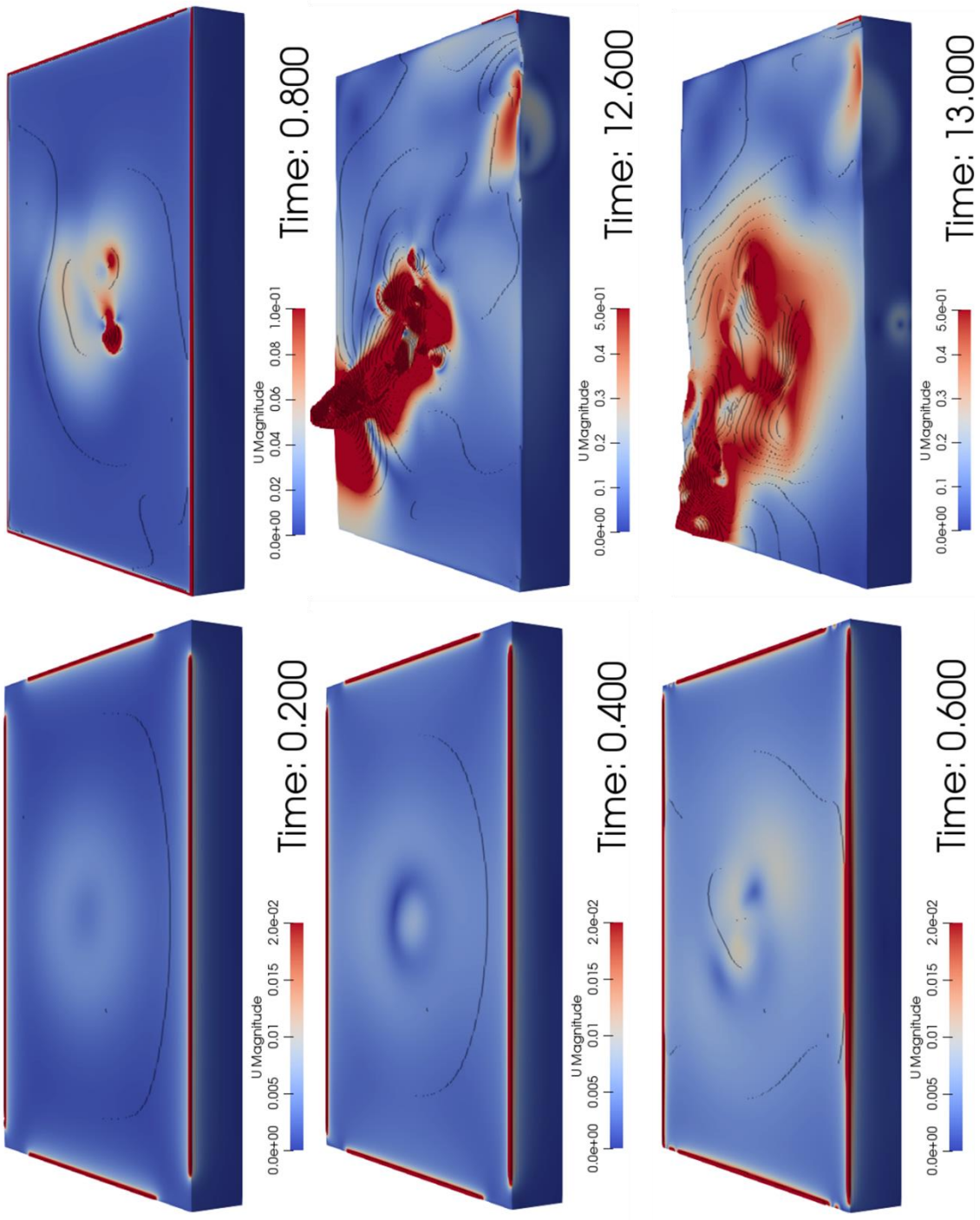

Annex T. Free surface visualization and velocity field for simulation of LP2 tank with deflector.

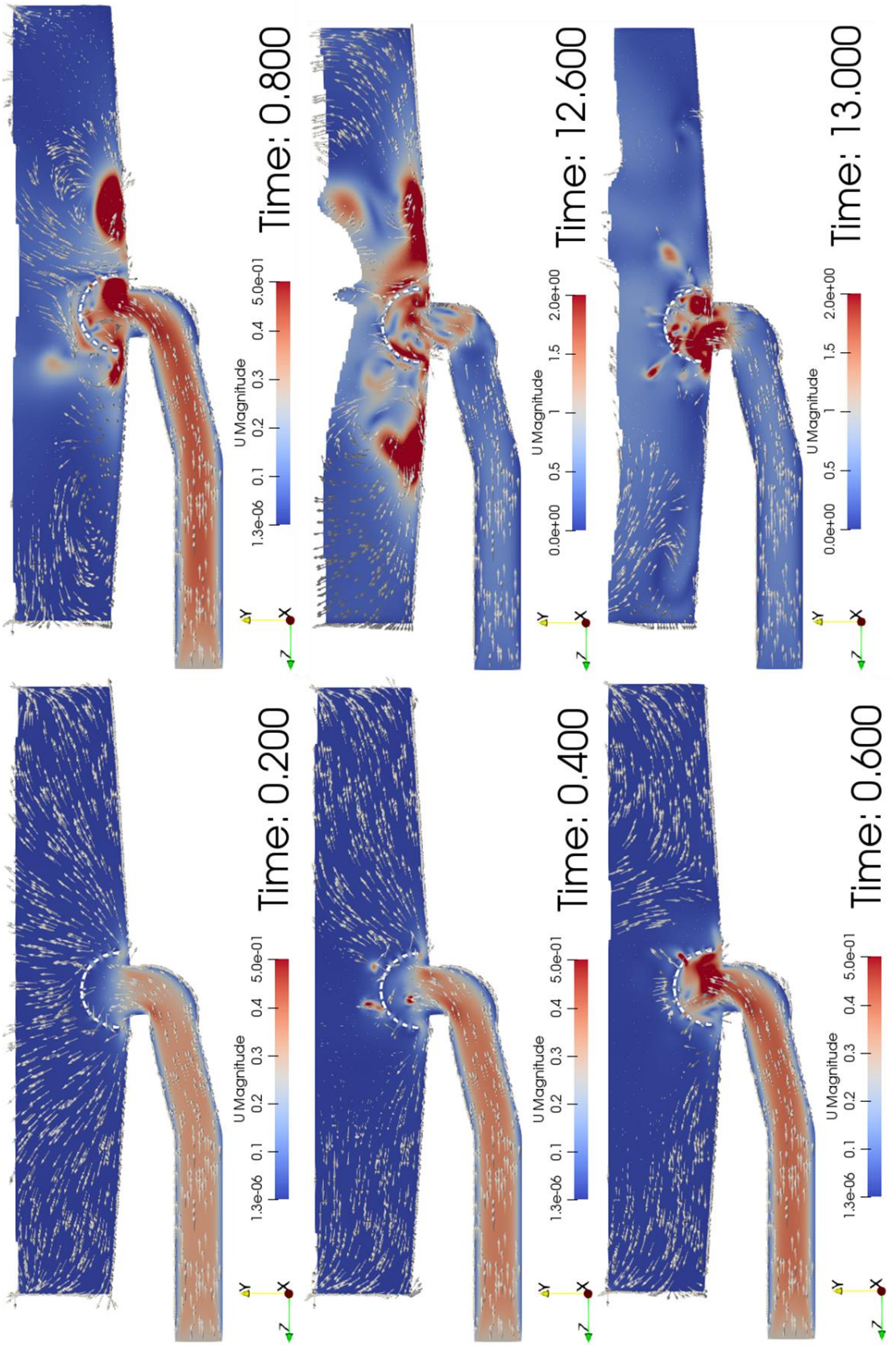

Annex U. Flow velocity visualization at the symmetry plane of the tank.